Honokiol ameliorates pyroptosis in intestinal ischemia-reperfusion injury by regulating the SIRT3-mediated NLRP3 inflammasome

KE WU[1], QIULING WANG[1], ZHENGYU ZHANG[1], WEI LUO[1], JING PENG[1], XIN MA[1], LI WANG[2], CHUNGUANG XIE[3] and WUBIN GUO[1,4]

[1]Department of General Surgery, The Affiliated Traditional Chinese Medicine Hospital, Southwest Medical University, Luzhou, Sichuan 646000, P.R. China; [2]Research Center of Integrative Medicine, The Affiliated Traditional Chinese Medicine Hospital, Southwest Medical University, Luzhou, Sichuan 646000, P.R. China; [3]Traditional Chinese Medicine Regulating Metabolic Diseases Key Laboratory of Sichuan Province, Hospital of Chengdu University of Traditional Chinese Medicine, Chengdu, Sichuan 610075, P.R. China; [4]The Key Laboratory of Integrated Traditional Chinese and Western Medicine for Prevention and Treatment of Digestive System Diseases of Luzhou City, The Affiliated Traditional Chinese Medicine Hospital, Southwest Medical University, Luzhou, Sichuan 646000, P.R. China

Received August 11, 2024; Accepted March 11, 2025

DOI: 10.3892/ijmm.2025.5537

Abstract. Intestinal ischemia-reperfusion (IIR) injury is caused by the restoration of blood supply after a period of ischemia. It occurs in numerous clinical pathologies, such as intestinal obstruction, incarcerated hernia and septic shock, with mortality rates of 50-80%. Honokiol (HKL), isolated from the herb *Magnolia officinalis*, is a biphenolic natural product with antioxidative, antibacterial, antitumor and anti-inflammatory properties. Additionally, HKL has protective effects in ischemia-reperfusion injuries, but its role and specific mechanisms in IIR injury are yet to be elucidated. In the present study, the superior mesenteric artery was ligated in rats to establish an IIR model. Hematoxylin and eosin staining and ELISA revealed that HKL administration ameliorated IIR-induced injury in rats, which was demonstrated by a reduced destruction to the intestinal mucosa, as well as a reduced serum intestinal fatty acid-binding protein concentration and Chiu's score in 10 mg/kg HKL treated IIR-induced rats compared with those without HKL treatment. Additionally, immunohistochemical (IHC) staining and western blotting revealed that the occludin and tight junction protein 1 protein levels were increased in the 10 mg/kg HKL treated IIR-induced rats compared with those without HKL treatment. Furthermore, an *in vitro* hypoxia/reoxygenation (H/R) cell model was established using IEC-6 cells. Cell Counting Kit-8 and lactate dehydrogenase (LDH) assays indicated that HKL mitigated the H/R-inhibited cell viability and decreased the LDH levels in cell supernatants. Mechanistically, immunofluorescent (IF) staining and western blotting revealed that HKL inhibited H/R-triggered pyroptosis. Furthermore, Mito-Tracker, mitochondrial membrane potential and MitoSOX staining as well as western blotting revealed that reducing mitochondrial reactive oxygen species (ROS) inhibited the H/R-induced pyroptosis by mitigating mitochondrial dysfunction. In the present H/R cell model, HKL improved the mitochondrial function by increasing the expression of sirtuin 3 (SIRT3), while IF staining and western blotting indicated that silencing SIRT3 notably reduced the beneficial effect of HKL on pyroptosis. In addition, IHC staining and western blotting revealed that HKL treatment mitigated the IIR-induced pyroptosis in rats. Therefore, HKL treatment may mitigate IIR-induced mitochondrial dysfunction and reduce mitochondrial ROS production by increasing the expression of SIRT3 protein, potentially resulting in an inhibition of pyroptosis during IIR.

Correspondence to: Professor Chunguang Xie, Traditional Chinese Medicine Regulating Metabolic Diseases Key Laboratory of Sichuan Province, Hospital of Chengdu University of Traditional Chinese Medicine, 39 Shierqiao Road, Chengdu, Sichuan 610075, P.R. China
E-mail: xcg718@aliyun.com

Dr Wubin Guo, Department of General Surgery, The Affiliated Traditional Chinese Medicine Hospital, Southwest Medical University, 182 Chunhui Road, Luzhou, Sichuan 646000, P.R. China
E-mail: gwb0127@163.com

Key words: honokiol, pyroptosis, intestinal ischemia-reperfusion, sirtuin 3, NOD-, LRR- and pyrin domain-containing protein 3

Introduction

Intestinal ischemia-reperfusion (IIR) is an acute condition often caused by cardiopulmonary bypass, small intestinal transplantation, intestinal obstruction, mesenteric ischemia, incarcerated hernia, septic shock or trauma with a mortality rate of >50% and a global incidence rate of >0.001% (1-3). In America, 30,000 individuals per year experience ischemia-reperfusion (4). Furthermore, acute mesenteric ischemia alone accounts for 0.1% of all hospital admissions globally (5). Despite improvements in treatment modalities, the mortality rate of acute mesenteric ischemia is 50-80% (5). Therefore, investigating novel therapeutic strategies to improve the treatment of IIR is necessary.

During IIR, epithelial cell death and mucosal injury disrupts the integrity of the mucosal barrier, which increases intestinal permeability, resulting in systemic inflammatory response syndrome or shock (6,7). Previous studies have shown that non-apoptotic cell death mechanisms, including ferroptosis, pyroptosis and necroptosis, serve key roles in the pathological process of acute and chronic gut injury (8,9).

Pyroptosis, a type of proinflammatory programmed cell death, occurs in multiple types of cells, such as enterocytes, oligodendrocytes and vascular endothelial cells including those in the digestive system, under several stress conditions such as mitochondrial oxidative stress and endoplasmic reticulum stress, and in response to a large number of metabolites such as trimethylamine N-oxide and methylglyoxal (10-13). Pyroptotic cells release several inflammatory cytokines and danger-associated molecular patterns (DAMPs) through gasdermin D (GSDMD) pores or ruptured membranes, resulting in the activation of immune cells such as alveolar macrophages and non-immune cells such as lung endothelial cells that in turn generate further proinflammatory cytokines (10). This exacerbates inflammation and induces further pyroptosis, which leads to a positive feedback loop and host mortality (10,14). For example, interleukin (IL)-1β and IL-18, released from pyroptotic cells, recruit and activate immune cells by binding to IL-receptors. This triggers the production of several proinflammatory cytokines, such as tumor necrosis factor-α (TNF-α) and interferon-γ (IFN-γ), which amplifies the proinflammatory response (10). IFN-γ and TNF-α induce pyroptosis and inflammatory responses through the activation of the janus kinase/signal transducer and activator of transcription 1/IFN regulatory factor 1 pathway. However, blocking the activation of IFN-γ and TNF-α using neutralizing antibodies ameliorates infectious and autoinflammatory diseases by inhibiting inflammation and tissue damage (15,16). In addition, as a DAMP, high-mobility group box 1 not only activates macrophages to generate inflammatory cytokines, but it also induces pyroptosis in macrophages, which further exacerbates the inflammatory response (14,17). Therefore, the initiation of excessive pyroptosis leads to severe inflammatory consequences, whereas its inhibition ameliorates the pathogenic effects of inflammatory diseases. It is generally accepted that the NOD-, LRR- and pyrin domain-containing protein 3 (NLRP3) inflammasome, which is an inflammatory regulatory complex, contributes to the initiation of pyroptosis (18-20). Once the assembly of inflammasomes is complete, procaspase-1 is recruited and cleaved, and then its active fragment not only cleaves pro-IL-1β and pro-IL-18 into their activated forms but it also transforms GSDMD into C- and N-terminal fragments, which triggers pyroptosis (21,22). In addition, previous studies demonstrate that NLRP3-GSDMD-dependent pyroptosis contributes to IIR injury (23-25). Therefore, inhibiting NLRP3 pathway-mediated pyroptosis might be a promising therapeutic option for IIR injury.

Mitochondrial dysfunction is considered to be one of the principal contributors to IIR-induced injury. When IIR occurs, mitochondria inhibit adenosine triphosphate generation, produce reactive oxygen species (ROS) and increase the amount of mitochondrial DNA (mtDNA) in the blood circulation, thereby aggravating cell damage (26,27). Recent studies reveal that mitochondrial dysfunction contributes to NLRP3 inflammasome activation-induced pyroptosis during pathological processes, such as septic shock and hepatic encephalopathy (28,29). Mitochondria-associated membrane formation during IIR activates the NLRP3 inflammasome and induces pyroptosis (30). Therefore, mitochondrial dysfunction may contribute to NLRP3 inflammasome activation-induced pyroptosis in IIR injury. Sirtuin-3 (SIRT3), which is mainly expressed in mitochondria, is usually reduced in models of IR, including IIR (31-33). The activation of SIRT3 protects against IIR injury by ameliorating mitochondrial damage (34). However, whether SIRT3 can ameliorate NLRP3 inflammasome activation-triggered pyroptosis by regulating mitochondrial function during IIR has not been fully elucidated.

Honokiol (HKL), a natural small-molecule polyphenol extracted from the herb *Magnolia officinalis*, has been identified to possess antitumor, anti-inflammatory and antioxidant properties (35-37). Furthermore, HKL can directly target SIRT3 and increase SIRT3 expression levels (38). A previous study demonstrates that HKL can protect mitochondrial integrity by activating SIRT3 in cisplatin-induced acute kidney injury (39,40). Therefore, the present study investigated whether HKL can also ameliorate IIR injury. Subsequently, the present study investigated the underlying mechanisms of HKL and its effects on IIR in a rat model of small IIR and in IEC-6 epithelial cells.

Materials and methods

Rat model of small IIR. In total, 96 8-week-old adult male Sprague-Dawley rats [Shanghai Jihui Laboratory Animal Breeding Co.,Ltd.; license no. SCXK(Hu)2022-0009] weighing 250-300 g were kept in an environment with a stable humidity (40-70%) and temperature (22±2˚C), with a time-controlled lighting system and unrestricted access to water and standard commercial food. The time-controlled lighting system had a 12 h light/dark cycle. All animal experimental protocols were approved by the ethics committee of the Southwest Medical University (Luzhou, China; approval no. 20221128-001). After the rats had adapted to their environment for 5 days, 24 rats were used to investigate different durations of ischemia to determine the duration that gave the most notable alteration in intestinal damage after IIR. The rats were randomly divided into groups (n=6/group), namely: The sham; ischemia for 30 min and reperfusion for 2 h; ischemia for 45 min and reperfusion for 2 h; or ischemia for 60 min and reperfusion for 2 h groups. The rat IIR model was established as previously described (41,42). Prior to surgery, a mixture containing ketamine (55 mg/kg) and xylazine (7.5 mg/kg) was injected once to anesthetize the rats via intraperitoneal injection (duration, ~70 min). To ensure that the rats were anesthetized, 1 min after injection the rats were rolled onto their sides once every min until the righting reflex was lost. Subsequently, 1 min after the righting reflex was lost, a toe pinch test was applied to each rat to determine whether the withdrawal reflex was present. Loss of the righting reflex and toe pinch response was used to confirm that the rats were anesthetized. A midline laparotomy was carried out, and then the superior mesenteric artery (SMA) was exposed and clamped for 30, 45 or 60 min at 22±2˚C. During the surgical period and ischemia, a tail pinch test was carried

out once every 5 min and the palpebral reflex was observed to monitor the degree of anesthesia. If the rats reacted to the tail pinch test or the palpebral reflex was observed, anesthesia was maintained with injections of 20 mg/kg ketamine. After ischemia, the clamp was removed, and the skin was sutured after the intestines returned to a pink color. Subsequently, reperfusion was performed for 2 h, and the rats were allowed to wake up. In the sham group, the rats underwent the same procedure without SMA occlusion. In the subsequent experiments, the SMA was clamped for 45 min at 22±2˚C, and 42 rats were randomly divided into seven groups (n=6/group) to determine the appropriate dose of HKL, namely: The sham; IIR; IIR with 0.5 mg/kg HKL (MedChemExpress) (IIR + 0.5 HKL); IIR with 1 mg/kg HKL (IIR + 1 HKL); IIR with 5 mg/kg HKL (IIR + 5 HKL); IIR with 10 mg/kg HKL (IIR + 10 HKL); or IIR with 20 mg/kg HKL (IIR + 20 HKL) groups. In addition, 30 rats were randomly divided into three groups (n=10/group),namely: The sham; IIR; and IIR + 10 HKL groups, which were used for immunohistochemical (IHC), intestinal fatty acid-binding protein (i-FABP), IL-1β and IL-18 tests (n=6/group) or western blotting tests (n=4/group). For the HKL treatment groups, a solvent mixture of DMSO and PBS at a volume ratio 1:1 was prepared. HKL was dissolved in the solvent mixture to prepare a 10 mg/ml stock solution. The HKL stock solution was added to the solvent mixture of DMSO and PBS to prepare working solutions according to the injection dose and total mass of each rat. Each rat was administered an intraperitoneal injection of 1 ml HKL solution once daily for 7 days prior to surgery (43-45). All animals from the sham and IIR groups were given an equal volume of the solvent mixture of DMSO and PBS via an intraperitoneal injection. Following reperfusion, rats were anesthetized using a mixture of ketamine (55 mg/kg) and xylazine (7.5 mg/kg), and peripheral blood was collected from the abdominal aorta to euthanize all animals. Rats were confirmed dead when the absence of a heartbeat, pulse, breathing and corneal reflex was observed for >3 min. The rats were then dissected, and the small intestine collected.

Hematoxylin and eosin (H&E) staining and pathological score. For pathological experiments, all of the small intestinal tissues were fixed in 4% polyformaldehyde for 24 h at 4˚C and embedded in paraffin. Following cooling at -20˚C, 4 μm-thick sections were prepared using a tissue slicer and stained with H&E solution (cat. no. G1005-500ML; Wuhan Servicebio Technology Co., Ltd.). The sections were stained using hematoxylin for 5 min at room temperature. After washing with water, the sections were stained using eosin for 15 sec at room temperature. Following staining, the morphology of the small intestine was observed using a light microscope (magnification, x100; Eclipse E100; Nikon Corporation). The destruction of the small intestinal tissues was evaluated using Chiu's score (46) and ImageJ software (version 1.8.0; National Institutes of Health). Two independent observers blinded to the groups determined the Chiu's score.

IHC staining. Small intestinal tissues were fixed in 4% polyformaldehyde for 24 h at 4˚C and embedded in paraffin. Following cooling at -20˚C, sections (4 μm-thick) of intestinal tissue were prepared and dewaxed using BioDewax and Clear Solution (cat. no. G1128-500ML; Wuhan Servicebio Technology Co., Ltd.) and hydrated in ethanol at different concentrations. Following antigen retrieval for 20 min at 95˚C, the tissue sections were incubated with 3% BSA (cat. no. GC305010-5 g; Wuhan Servicebio Technology Co., Ltd.) for 30 min at room temperature. Subsequently, the tissues were incubated with primary antibodies: Anti-tight junction protein 1 (ZO-1; 1:250; cat. no. 164329; Chengdu Zen-Bioscience Co., Ltd.); anti-occludin (1:250; cat. no. 502601; Chengdu Zen-Bioscience Co., Ltd.); anti-NLRP3 (1:300; cat. no. GB114320-100; Wuhan Servicebio Technology Co., Ltd.); anti-SIRT3 (1:100; cat. no. GB115590-100; Wuhan Servicebio Technology Co., Ltd.); anti-cleaved-Caspase-1 (cleavedCleaved-Casp1; 1:200; cat. no. YC0003; ImmunoWay Biotechnology Company); and anti-GSDMD N-terminal domain (GSDMD-N; 1:100; cat. no. DF13758; Affinity Biosciences) at 4˚C overnight. The tissue samples were then incubated with a HRP-conjugated goat anti-rabbit secondary antibody (1:1,000; cat. no. GB23303; Wuhan Servicebio Technology Co., Ltd.) at room temperature for 50 min and visualized using a DAB substrate chromogen kit (cat. no. G1212-200T; Wuhan Servicebio Technology Co., Ltd.), after the cell nuclei were stained with hematoxylin solution for 5 min at room temperature. All images were captured using an inverted light microscope (magnification, x100 and x400; OLYMPUS IX73; Olympus Corporation) and analyzed using ImageJ software (version 1.8.0; National Institutes of Health).

Hypoxia/reoxygenation (H/R) model and treatments. A rat intestinal IEC-6 epithelial cell line was provided by Wuhan Sunncell Biotechnology Co., Ltd. IEC-6 cells were cultured in DMEM (cat. no. 11965092; Thermo Fisher Scientific, Inc.) with 10% FBS (cat. no. 13011-8611;Zhejiang Tianhang Biotechnology Co., Ltd.) and 10 mg/l insulin at 37˚C in a 5% CO_2 atmosphere.

To establish the H/R model *in vitro*, IEC-6 cells were maintained in a Water-Jacketed CO_2 incubator commercial hypoxia system (Thermo Scientific™ 8000; Thermo Fisher Scientific, Inc.; 94% N_2, 5% CO_2 and 1% O_2) for 12 h at 37˚C. Following hypoxia, IEC-6 cells were transferred to a normoxic incubator (74% N_2, 5% CO_2 and 21% O_2) and further cultured for 6 h at 37˚C (47). For the treatment groups, a solvent mixture of DMSO and PBS at a 1:1 volume ratio was prepared. HKL was dissolved in the solvent mixture to prepare a 10 mM stock solution. The HKL stock solution was then further diluted in the solvent mixture of DMSO and PBS to prepare working solutions according the dose and total volume required. The mitochondria-targeted antioxidant (Mito-TEMPO; MedChemExpress) was dissolved in deionized water. HKL (1, 5, 10, 20 or 40 μM) or Mito-TEMPO (200 μM) solutions were used to treat cells at 37˚C for 12 h prior to H/R.

Cell transfection. Small interfering (si)-RNA targeting SIRT3 mRNA (siSIRT3; sense, 5'-GGACGGAUAAGACAGACU AUGDTDT-3'; antisense, 5'-CAUAGUCUGUCUUAUCCGU CCDTDT-3'; Shanghai GenePharma Co., Ltd.) and the scrambled negative control (con) siRNA (siNC; sense, 5'-ACGUGG GAGAAGAUCGUACAADTDT-3'; antisense, 5'-UUGUAC GAUCUUCUCCCACGUDTDT-3'; Shanghai GenePharma Co., Ltd.) were transfected into cells using Lipofectamine®

2000 (cat. no. 11668019; Thermo Fisher Scientific, Inc.). Briefly, IEC-6 cells ($6x10^5$ cells/well) were seeded in a 6-well plate at 37˚C overnight for attachment before being transfected using 12.5 μl of Lipofectamine® 2000 with 25 nM siSIRT3 or siNC for 48 h at 37˚C. After transfection, cells were immediately used for subsequent experiments.

Reverse transcription-quantitative polymerase chain reaction (RT-qPCR). After exposure to H/R and HKL, IEC-6 cells were collected and treated with TRIzol® reagent (cat. no. 15596-026; Thermo Fisher Scientific, Inc.). Reverse transcription was performed using M-MLV Reverse Transcriptase (cat. no. 28025013; Thermo Fisher Scientific, Inc.) at 42˚C for 1 h and 70˚C for 10 min. qPCR was performed using TB Green Fast qPCR Mix (cat. no. RR430A; Takara Biotechnology Co., Ltd.) under the following conditions: Initial denaturation at 95˚C for 15 sec; followed by 40 cycles of 95˚C for 5 sec and 60˚C for 30 sec. β-actin was used as a con. The relative expression of SIRT3 mRNA was calculated using the $2^{-\Delta\Delta cq}$ method (48). The primer sequences used in the present study were: SIRT3 forward, 5'-GCCTCTACAGCA ACCTTC-3' and reverse, 5'-AAGTAGTGAGCGACATTG G-3'; β-actin forward, 5'-CCATTGAACACGGCATTG-3' and reverse, 5'-TACGACCAGAGGCATACA-3'.

Western blotting. To extract total protein, IEC-6 cells or small intestinal tissues were treated with RIPA buffer (cat. no. F1053; Wuhan Frekang Technology Co., Ltd. The protein concentration was determined using a BCA protein assay kit (cat. no. K001; Wuhan Fine Biotech Co., Ltd.). Following separation using 10% SDS-PAGE (20 μg of total protein loaded per lane), the proteins were transferred to a PVDF membrane (cat. no. 36126ES; Shanghai Yeasen Biotechnology Co., Ltd.) and blocked using 5% non-fat milk for 2 h at room temperature. The membrane was incubated with primary antibodies at 4˚C overnight. The primary antibodies used were: Anti-ZO-1 (1:500; cat. no. GB111402-100; Wuhan Servicebio Technology Co., Ltd.); anti-occludin (1:800; cat. no. GB11149-50; Wuhan Servicebio Technology Co., Ltd.); anti-SIRT3 (1:300; cat. no. GB115590-100; Wuhan Servicebio Technology Co., Ltd.); anti-NLRP3 (1:400; cat. no. GB114320-100; Wuhan Servicebio Technology Co., Ltd.); anti-cleaved-Casp1 (1:800; cat. no. AF4005; Affinity Biosciences); anti-Casp1 (1:1,000; cat. no. AF5418; Affinity Biosciences); anti-GSDMD (1:500; cat. no. GB114198-50; Wuhan Servicebio Technology Co., Ltd.); anti-GSDMD-N (1:900; cat. no. DF13758; Affinity Biosciences); and anti-β-actin (1:4,000; cat. no. 30102ES60; Shanghai Yeasen Biotechnology Co., Ltd.). Following washing with tris buffered saline with tween (0.05%), the membranes were treated with a HRP-conjugated secondary antibody (1:10,000; cat. no. GB23303; Wuhan Servicebio Technology Co., Ltd.) at room temperature for 1 h. The target signals were visualized using a super ECL detection kit (cat. no. 36208ES60; Shanghai Yeasen Biotechnology Co., Ltd.) and quantified using ImageJ software (version 1.8.0; National Institutes of Health).

i-FABP, IL-1β and IL-18 assay. Levels of i-FABP in the serum and culture supernatant as well as serum IL-1β and IL-18 levels were analyzed using rat i-FABP ELISA (cat. no. CSB-E08026r; Cusabio Technology, LLC), rat IL-1β ELISA (cat. no. CSB-E08055r; Cusabio Technology, LLC) and rat IL-18 ELISA (cat. no. CSB-E04610r; Cusabio Technology, LLC) kits (49). The standards and samples were incubated with the biotin-conjugated antibody for 1 h at 37˚C, followed by an incubation with HRP-streptavidin for 1 h at 37˚C. The tetramethylbenzidine substrate was subsequently added to all wells. After terminating the reaction, the absorbance of each well was tested using a microplate reader (Berthold Tristar2 S LB 942) at 450 nm.

Lactate dehydrogenase (LDH) assay. LDH levels in cell supernatants from each treatment group were tested using a LDH assay kit (cat. no. C0016; Beyotime Institute of Biotechnology). Briefly, cell culture plates were centrifuged at 400 x g for 5 min at room temperature, and the culture supernatants were obtained. The culture supernatants of IEC-6 cells were treated with the LDH detection working solution for 30 min at room temperature in a darkroom. The absorbance was then determined using a microplate reader (Berthold Tristar2 S LB 942) at 490/630 nm.

Cell viability assay. A Cell Counting Kit-8 (CCK-8; cat. no. C0037; Beyotime Institute of Biotechnology) was used to determine IEC-6 cell viability. Briefly, IEC-6 cells ($4.5x10^3$ cells/well) were seeded in a 96-well plate for 24 h at 37˚C. Following hypoxia for 12 h and reoxygenation for 6 h at 37˚C, 10 μl of CCK-8 solution was added for 1 h. Subsequently, the absorbance of each group was analyzed using a microplate reader (Berthold Tristar2 S LB 942) at 450 nm.

Immunofluorescent (IF) staining. Following hypoxia for 12 h and reoxygenation for 6 h at 37˚C, IEC-6 cells were fixed with cold 4% paraformaldehyde solution for 25 min at 4˚C, followed by permeabilization with 1% Triton X-100 working solution. The cells were then treated with 3% BSA (cat. no. GC305010-5g; Wuhan Servicebio Technology Co., Ltd.) at room temperature for 45 min. Anti-NLRP3 (1:300; cat. no. GB114320-100; Wuhan Servicebio Technology Co., Ltd.); anti-cleaved-Casp1 (1:100; cat. no. YC0003; ImmunoWay); or anti-GSDMD-N (1:200; cat. no. DF13758; Affinity Biosciences) antibodies were incubated with cells at 4˚C overnight. Subsequently, an Alexa Fluor® 488-conjugated secondary antibody (1:400; cat. no. GB25303; Wuhan Servicebio Technology Co., Ltd.) was added for 1 h at 37˚C. Cell nuclei were stained using a DAPI solution (cat. no. G1012; Wuhan Servicebio Technology Co., Ltd.) for 10 min at room temperature. All images were captured using an Eclipse C1 Nikon fluorescence microscope (magnification, x200; Nikon Corporation).

Mitochondrial morphology and mitochondrial membrane potential ($\Delta\psi_m$) analysis. To assess mitochondrial morphology, IEC-6 cells were washed and stained with Mito-Tracker Green (final concentration, 100 nM; cat. no. C1048; Beyotime Institute of Biotechnology) for 20 min at 37˚C. An A1+R Nikon confocal microscope(Nikon Corporation)was then used to observe mitochondrial morphology (magnification, x1,000).

For the $\Delta\psi_m$ analysis, IEC-6 cells were labeled with 1 ml of tetramethylrhodamine ethyl ester perchlorate solution (final concentration, 10 μM; cat. no. C2001S; Beyotime Institute

of Biotechnology) at 37˚C for 35 min. Following washing, the $\Delta\psi_m$ was determined using an Eclipse C1 Nikon fluorescence microscope (magnification, x200; Nikon Corporation).

Mitochondrial ROS analysis. To assess mitochondrial ROS, IEC-6 cells were co-labeled with MitoSOX Red (final concentration, 5 μM; cat. no. S0061S; Beyotime Institute of Biotechnology) and Mito-Tracker Green (final concentration, 100 nM; cat. no. C1048; Beyotime Institute of Biotechnology) for 20 min at 37˚C. Microscopy images were captured using an Eclipse C1 Nikon fluorescence microscope (magnification, x400; Nikon Corporation).

Statistical analysis. Statistical data were analyzed using SPSS software (version 19.0; IBM Corp.). Data are presented as the mean ± SD. Statistical graphs were created using GraphPad Prism (version 5; GraphPad; Dotmatics). Difference comparisons between groups were performed using an unpaired Student's t-test or one-way ANOVA followed by Tukey's post hoc test. $P<0.05$ was considered to indicate a statistically significant difference.

Results

HKL alleviates IIR-induced intestinal injury in rats. To produce an appropriate rat IIR model, the SMA was clamped for 30, 45 or 60 min, followed by reperfusion for 2 h according to previously described methods (41,42). The results revealed that the most evident alterations in intestinal damage were observed in the rats after 45 min of ischemia and 2 h of reperfusion, as demonstrated by an increased Chiu's score (Fig. S1). Therefore, 45 min of ischemia and 2 h of reperfusion was used to induce IIR injury in rats for the subsequent *in vivo* experiments.

To determine the beneficial effects of HKL (Fig. 1A) treatment on IIR-induced intestinal injury, five different doses of HKL (0.5, 1, 5, 10 or 20 mg/kg) were used once daily for 7 days prior to surgery (Fig. 1B) based on a previously published study (50). The results revealed that the pretreatment of rats with HKL at doses of 0.5, 1, 5, 10 or 20 mg/kg before IIR-induced injury, significantly reduced the damage to the intestinal mucosa and reduced the Chiu's score compared with that of the IIR-only group. In addition, the rats that were pretreated with 10 or 20 mg/kg HKL had reduced damage to the intestinal mucosa as well as a reduced Chiu's score compared with those of the 0.5, 1 or 5 mg/kg HKL pretreated rats (Fig. 1C and D). However, 20 mg/kg HKL did not have a significant effect on improving the damage in the Chiu score compared with that of HKL at the 10 mg/kg dose (Fig. 1C and D). Therefore, the 10 mg/kg HKL dose was used in the subsequent experiments. To further investigate the effect of HKL on IIR-induced intestinal injury, the concentration of serum i-FABP (a marker of tissue injury) was determined using ELISA. As shown in Fig. 1E, IIR injury significantly increased the concentration of serum i-FABP compared with the sham group. However, in rats with IIR-induced injury, HKL pretreatment significantly reduced the concentration of serum i-FABP compared with those without HKL pretreatment. In addition, the effect of HKL pretreatment on the small intestinal barrier was determined by analyzing occludin and ZO-1 protein expression levels using IHC staining and western blotting. The findings revealed that IIR-induced injury significantly reduced occludin and ZO-1 protein levels compared with those in the sham group. Furthermore, the reduced occludin and ZO-1 protein levels that were induced by IIR injury were significantly reversed with HKL pretreatment (Fig. 1F-H).

HKL alleviates H/R-triggered pyroptosis in IEC-6 cells. To investigate whether HKL had a beneficial role *in vitro*, the cytotoxicity of HKL on IEC-6 cells at five concentrations (1, 5, 10, 20 or 40 μM) was determined based on a previously published study (51). As shown in Fig. 2A, 40 μM HKL significantly reduced the viability of IEC-6 cells following treatment for 12 h. A H/R model was then established using IEC-6 cells, and a CCK-8 assay was used to investigate the effect of HKL treatment on cell viability. Compared with the con group, treatment with H/R significantly reduced the viability of IEC-6 cells. However, the viability of H/R treated IEC-6 cells was significantly increased after the cells were pretreated with 5, 10 and 20 μM HKL compared with those without HKL pretreatment (Fig. 2B). Therefore, 20 μM HKL was used for the subsequent experiments.

To further investigate whether HKL protected IEC-6 cells following H/R, the LDH (an index of cell injury) levels were analyzed. Compared with the con group, the LDH levels in the H/R group were significantly increased. Furthermore, the LDH levels in the IEC-6 cells treated with H/R and 20 μM HKL were significantly reduced compared with the cells that were only treated with H/R (Fig. 2C).

A number of studies show that pyroptosis serves an important role in IIR-induced injury (23,24). In addition, HKL inhibits NLRP3 inflammasome-mediated pyroptosis, which reduces lipopolysaccharide (LPS)-induced acute lung injury (50). Therefore, the present H/R model was used to determine whether HKL affected NLRP3 inflammasome-induced pyroptosis. Western blotting revealed that the GSDMD-N/GSDMD-full length (GSDMD-FL) ratio was increased in the H/R group compared with the con group. Furthermore, the GSDMD-N/GSDMD-FL ratio was significantly reduced in the 20 μM HKL pretreated H/R-induced cells compared with the H/R-induced cells without HKL pretreatment (Fig. 2D). IF staining experiments revealed that the protein expression of GSDMD-N was increased in the H/R group compared with the con group. However, the protein expression of GSDMD-N was reduced in the 20 μM HKL pretreated H/R-induced cells compared with the H/R-induced cells without HKL pretreatment (Fig. 2E). Additionally, the protein levels of NLRP3 and the cleaved-Casp1/Casp1-full length (Casp1-FL) ratio were significantly increased in the H/R group compared with those in the con group. Furthermore, the protein levels of NLRP3 and the cleaved-Casp1/Casp1-FL ratio were significantly decreased in the 20 μM HKL pretreated H/R-induced cells compared with the H/R-induced cells without HKL pretreatment (Fig. 2F). IF staining experiments indicated that the levels of NLRP3 and cleaved-Casp1 were increased in the H/R group compared with the con group. However, the levels of NLRP3 and cleaved-Casp1 were reduced in the 20 μM HKL pretreated H/R-induced cells compared with the H/R-induced cells without HKL pretreatment (Fig. 2G). Subsequently, the pyroptosis-related inflammatory products,

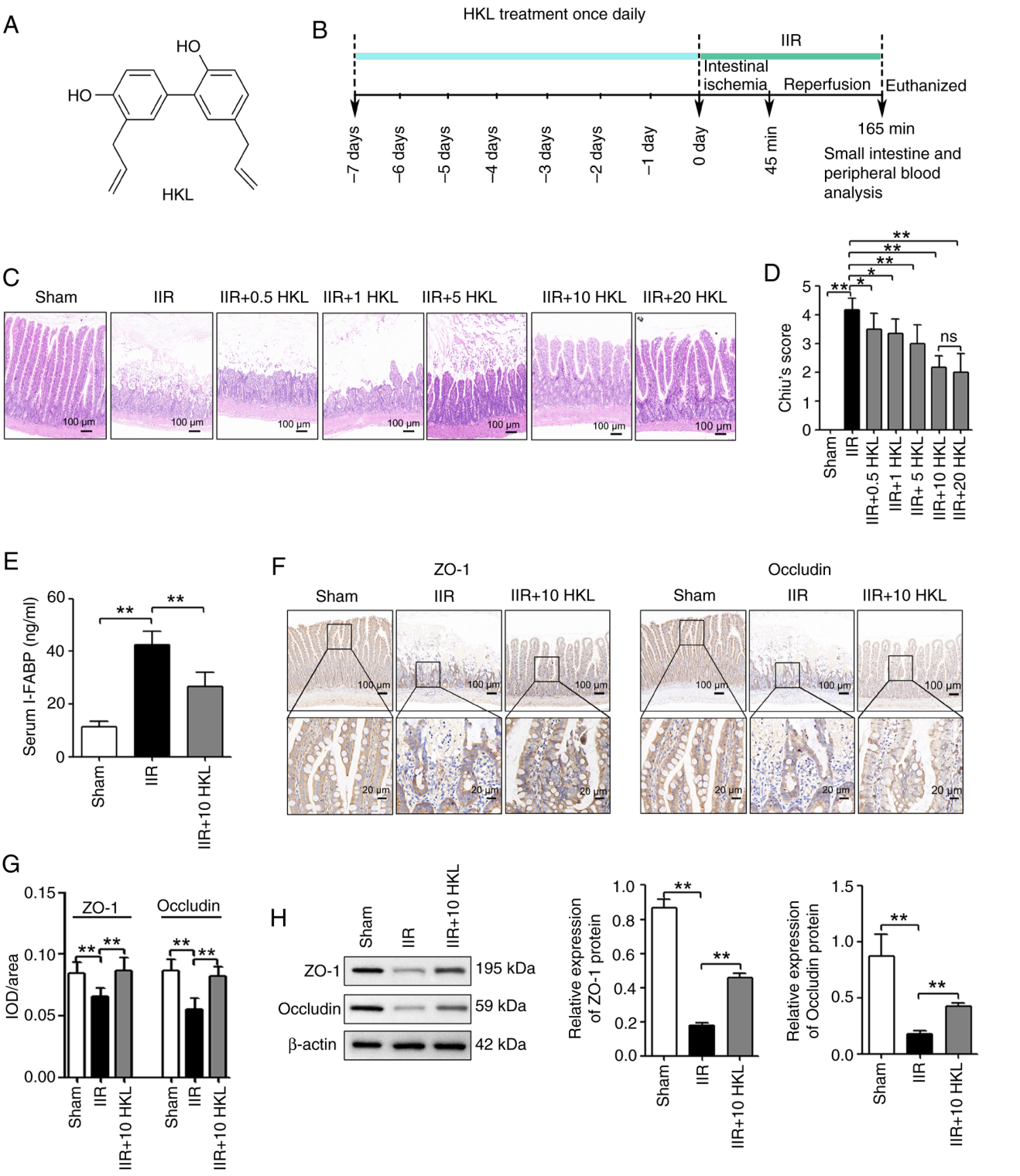

Figure 1. HKL treatment reduces IIR-induced intestinal injury in rats. (A) Chemical structure of HKL. (B) Workflow of the *in vivo* experiments. (C) Hematoxylin and eosin staining of intestinal tissues from rats after treatment with 0, 0.5, 1, 5, 10 or 20 mg/kg HKL (magnification, x100; scale bar, 100 μm). (D) Histopathological damage was determined using Chiu's score (n=6). (E) IIR-induced intestinal injury was measured using the serum i-FABP levels (n=6). (F) Consecutive sectioning of the same specimen for IHC staining was used to measure the protein expression levels of occludin and ZO-1 in the intestinal tissues of rats in different treatment groups (magnification, x100 or x400; scale bars, 100 or 20 μm; n=6). (G) Quantification of ZO-1 and occludin expression levels after IHC staining. (H) The protein expression levels of occludin and ZO-1 in the intestinal tissues of rats in different treatment groups were determined using western blotting (n=4). *P<0.05 and **P<0.01. ns, not significant; IHC, immunohistochemical; IIR, intestinal ischemia-reperfusion; HKL, honokiol; i-FABP, intestinal fatty acid-binding protein; ZO-1, tight junction protein 1; IOD, integrated optical density.

IL-1β and IL-18, were assessed. The results revealed that the IL-1β and IL-18 levels in the H/R group were significantly increased compared with those in the con group. However, the IL-1β and IL-18 levels were significantly reduced in the 20 μM HKL pretreated H/R-induced cells compared with the H/R-induced cells without HKL pretreatment (Fig. 2H).

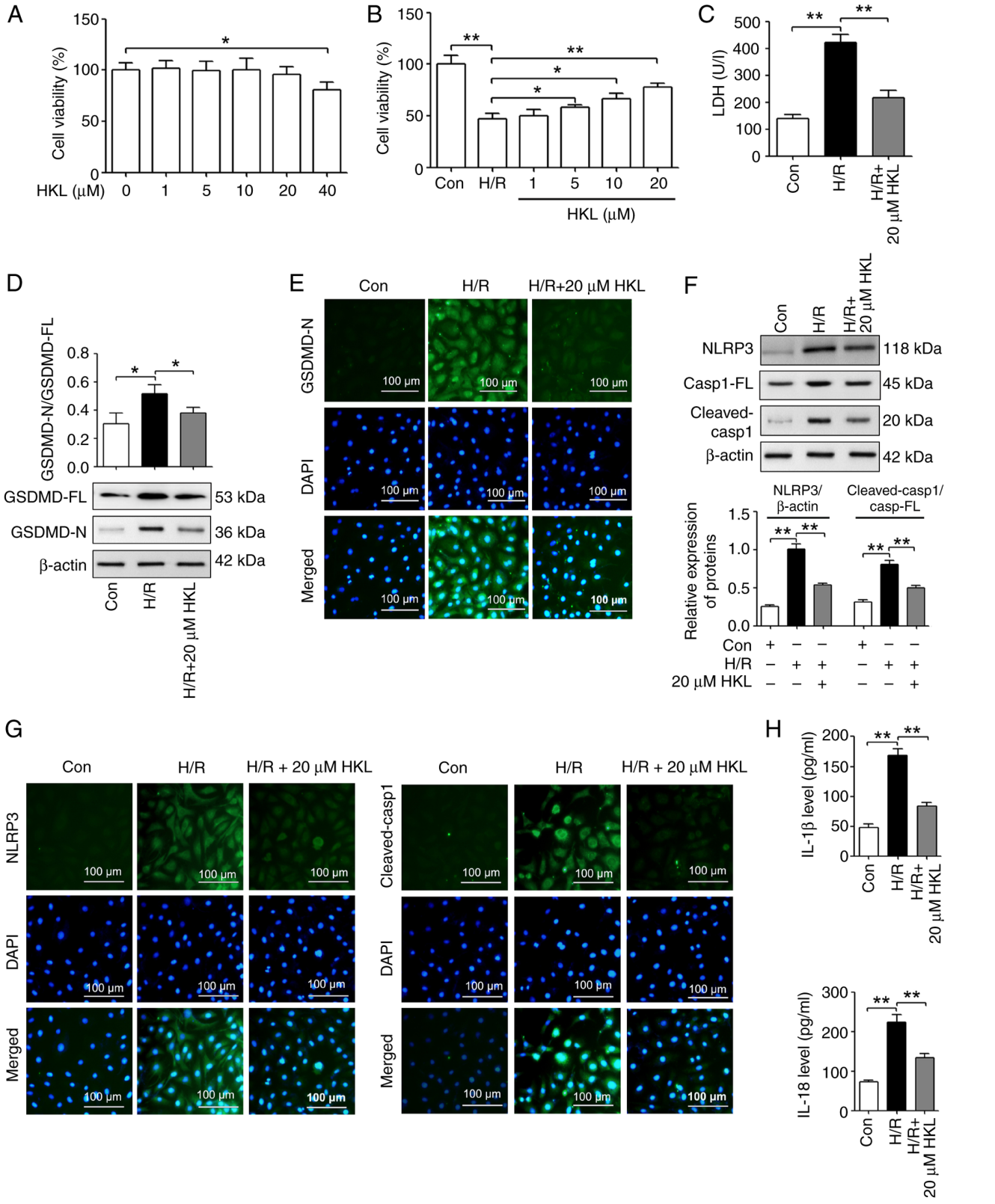

Figure 2. HKL treatment notably inhibits pyroptosis in IEC-6 cells following H/R. (A) HKL cytotoxicity to IEC-6 cells was measured using a CCK-8 assay (n=3). (B) The effect of HKL on the cell viability of H/R-treated IEC-6 cells was revealed using a CCK-8 assay (n=3). (C) The effect of HKL on cell injury was investigated by analyzing the LDH levels in cell supernatants from H/R-treated IEC-6 cells (n=3). (D) Western blotting assays were used to reveal the effect of HKL on GSDMD-FL and GSDMD-N expression levels in IEC-6 cells following H/R (n=3). (E) IF staining assays were used to demonstrate the effect of HKL on GSDMD-N expression levels in IEC-6 cells following H/R (magnification, x200; scale bar, 100 μm; n=3). (F) Western blotting assays were used to reveal the effects of HKL on the protein expression levels of NLRP3, Casp1-FL and cleaved-Casp1 in IEC-6 cells after H/R (n=3). (G) IF staining assays were used to demonstrate the effects of HKL on the expression levels of NLRP3 and cleaved-Casp1 in IEC-6 cells after H/R (magnification, x200; scale bar, 100 μm; n=3). (H) ELISA assays were used to reveal the effect of HKL on IL-1β and IL-18 protein levels in IEC-6 cells following H/R (n=3). *P<0.05 and **P<0.01. HKL, honokiol; LDH, lactate dehydrogenase; GSDMD, gasdermin D; GSDMD-FL, GSDMD-full length; GSDMD-N, GSDMD-N-terminal domain; H/R, hypoxia/reoxygenation; NLRP3, NOD-, LRR- and pyrin domain-containing protein 3; IF, immunofluorescent; IL, interleukin; Con, control; Casp1, caspase-1; Casp1-FL, Casp1-full length; CCK-8, Cell Counting Kit-8.

Inhibition of mitochondrial ROS alleviates H/R-triggered pyroptosis in IEC-6 cells. Previous studies reveal that mitochondrial dysfunction activates pyroptosis by regulating the $\Delta\psi_m$ and ROS production (52,53). Mitochondria are the predominant source of ROS production. To investigate the role of mitochondrial ROS in H/R-induced pyroptosis, mitochondrial ROS production was inhibited by Mito-TEMPO, which is a mitochondrion-targeted superoxide dismutase mimic that is usually used to scavenge superoxide and alkyl radicals (54). As shown in Fig. 3A, 200 μM Mito-TEMPO reduced the mitochondrial ROS production that was induced by H/R. Furthermore, mitochondrial fission was significantly increased in the H/R-induced IEC-6 cells compared with those in the con group. However, mitochondrial fission was significantly reduced in the Mito-TEMPO-treated H/R-induced cells compared with those without Mito-TEMPO treatment (Fig. 3B). In addition, H/R significantly reduced the $\Delta\psi$m in IEC-6 cells compared with the con group. This was significantly reversed in H/R-induced cells with Mito-TEMPO treatment (Fig. 3C).

Western blotting indicated that the GSDMD-N/GSDMD-FL ratio was significantly increased in the H/R group compared with the con group. However, Mito-TEMPO treatment significantly reversed this H/R-induced change (Fig. 3D). IF staining experiments demonstrated that the protein expression of GSDMD-N was increased in the H/R group compared with the con group, while Mito-TEMPO treatment reversed this H/R-induced change in the GSDMD-N levels (Fig. 3E). Additionally, western blotting assays revealed that Mito-TEMPO treatment significantly reversed the H/R-induced increases in the NLRP3 protein levels and cleaved-Casp-1/Casp-1-FL ratio (Fig. 3F). Furthermore, IF staining indicated that Mito-TEMPO treatment reversed the H/R-induced increases in NLRP3 and cleaved-Casp-1 protein levels (Fig. 3G). In addition, Mito-TEMPO treatment reversed the H/R-induced increases in the IL-1β and IL-18 protein levels (Fig. 3H).

HKL alleviates the H/R-induced mitochondrial dysfunction in IEC-6 cells. A previous study indicates that HKL alleviates amyotrophic lateral sclerosis by improving mitochondrial function and morphology (37). Therefore, the effect of HKL on mitochondrial dysfunction in the H/R model was investigated. MitoSOX Red and Mito-Tracker Green co-staining was carried out to evaluate the production of mitochondrial ROS. As shown in Fig. 4A, mitochondrial ROS generation was increased in H/R-induced IEC-6 cells compared with those in the con group. However, 20 μM HKL treatment reversed this H/R-induced increase in the ROS accumulation in the mitochondria. Mito-Tracker Green staining revealed that the mitochondrial fission was significantly increased in the H/R-treated IEC-6 cells compared with those in the con group, and 20 μM HKL treatment significantly reversed the H/R-induced increases in the mitochondrial fission and integrity (Fig. 4B). In addition, the H/R-induced reduction in the $\Delta\psi_m$ was significantly reversed with 20 μM HKL treatment (Fig. 4C).

HKL alleviates H/R-induced mitochondrial dysfunction by inducing the expression of SIRT3 protein in IEC-6 cells. SIRT3 is a mitochondrial protein that is involved in regulating mitochondrial function (55). In intracerebral hemorrhage, HKL protects mitochondrial function by increasing the expression of SIRT3 protein (40). Therefore, the effects of HKL treatment on SIRT3 in the present H/R cell model was investigated. SIRT3 levels were revealed to be significantly reduced in the H/R-induced cells compared with the con group. However, 20 μM HKL treatment significantly reversed the H/R-induced reduction in the SIRT3 levels (Fig. 5A). A previous study demonstrates that HKL also increases the mRNA expression of SIRT3 during cardiac hypertrophy (38). In the present study, 20 μM HKL treatment also increased the SIRT3 mRNA levels in IEC-6 cells after H/R inhibition (Fig. S2).

To determine whether siRNAs were transfected into IEC-6 cells, fluorescein amidite (FAM)-labeled siNC at doses of 25 and 50 μM was examined. As shown in Fig. 5B, cells were fluorescent after transfection with 25 and 50 μM FAM-labeled siNC, which indicated that transfection efficiency was >90%. As the transfection efficiency was comparable using 25 or 50 μM FAM-labeled siNC, siRNAs at doses of 25 μM were used for subsequent transfections. The knockdown efficiency of the SIRT3 siRNA was then examined. The results revealed that the expression of SIRT3 was significantly reduced in the siSIRT3 group compared with the siNC group (Fig. 5C).

To determine whether HKL affected mitochondrial function after H/R via SIRT3 in IEC-6 cells, SIRT3 levels were reduced using a SIRT3 specific siRNA (Fig. 5D). SIRT3 inhibition significantly reversed the HKL-induced differences in cell viability and LDH levels in the H/R model (Fig. 5E and F). Furthermore, the results demonstrated that HKL was unable to suppress the H/R-induced overproduction of mitochondrial ROS when SIRT3 was silenced in IEC-6 cells (Fig. 5G). Additionally, HKL treatment did not alleviate the H/R-induced mitochondrial fission in IEC-6 cells following SIRT3 silencing (Fig. 5H). In addition, HKL treatment reversed the H/R-induced reduction of the $\Delta\psi_m$ in IEC-6 cells; however, this HKL-induced increase in the $\Delta\psi_m$ was reduced when SIRT3 was silenced (Fig. 5I). Therefore, these results indicated that SIRT3 may be involved in the HKL-induced protection against mitochondrial dysfunction in the present H/R model.

HKL alleviates pyroptosis by increasing the expression of SIRT3 protein in H/R-induced cells. Due to the association between mitochondrial function and pyroptosis, the potential role of SIRT3 in the HKL-induced pyroptosis inhibition in IEC-6 cells was investigated. Fig. 6A shows that the HKL-induced reduction of the GSDMD-N/GSDMD-FL ratio was significantly reversed in the present H/R model following SIRT3 silencing. IF staining experiments also demonstrated that the HKL-induced reduction of GSDMD-N was reversed in the present H/R model following SIRT3 silencing (Fig. 6B). Additionally, the results revealed that the HKL-induced decrease in the NLRP3 protein levels and the cleaved-Casp1/Casp1-FL ratio in the present H/R model was significantly reversed following SIRT3 inhibition (Fig. 6C). IF staining experiments also demonstrated that the HKL-induced downregulation of NLRP3 and cleaved-Casp1 protein levels in the present H/R model were reversed following SIRT3 inhibition (Fig. 6D). In addition, HKL treatment significantly

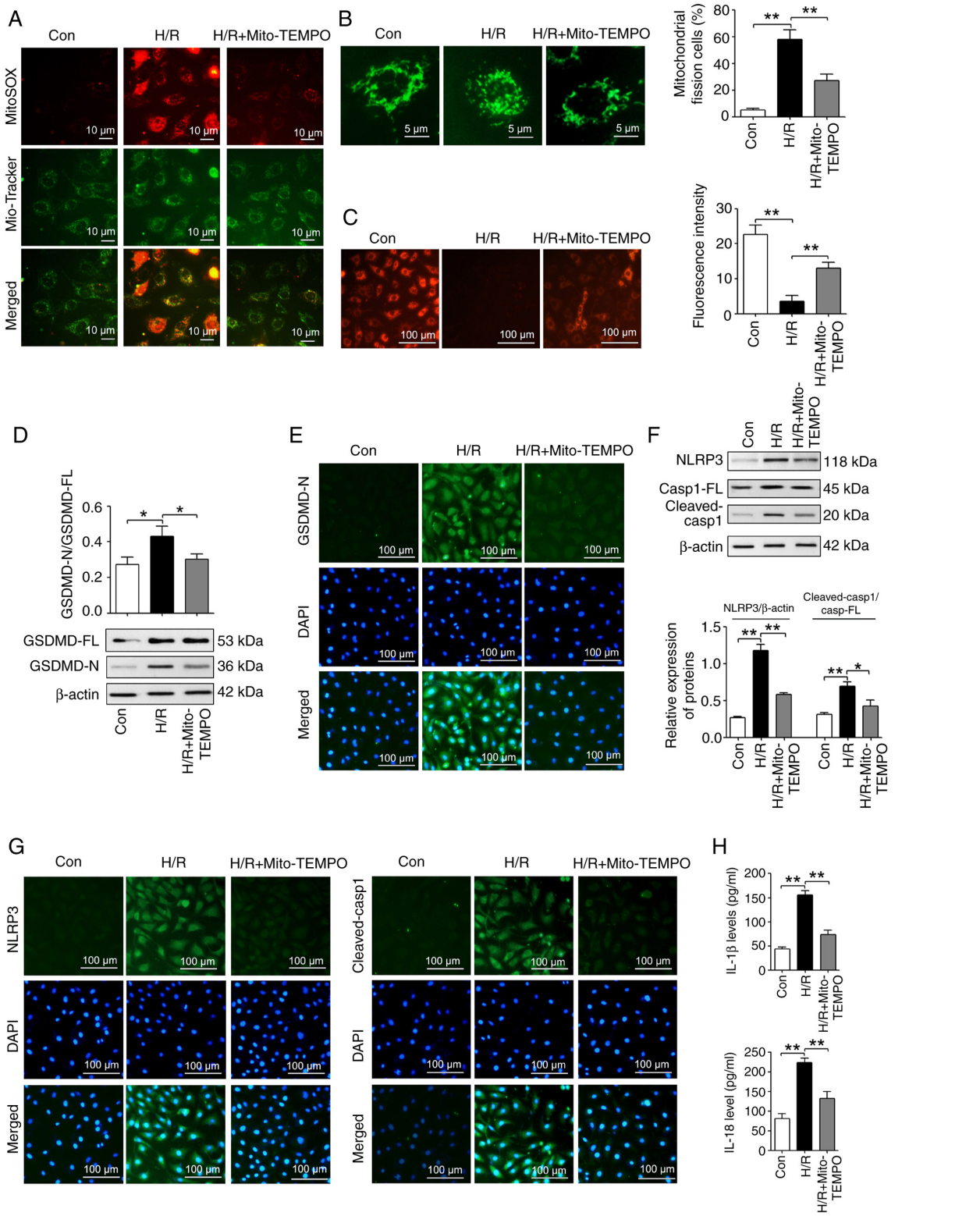

Figure 3. Inhibiting mitochondrial ROS with Mito-TEMPO reduces pyroptosis in IEC-6 cells following H/R. (A) MitoSOX Red and Mito-Tracker Green co-staining was used to analyze the production of mitochondrial ROS in different treatment groups (Mito-TEMPO, 200 μM; magnification, x400; scale bar, 10 μm). (B) Mitochondrial fission and integrity in different treatment groups were measured using Mito-Tracker Green staining (Mito-TEMPO, 200 μM; magnification, x1,000; scale bar, 5 μm; n=3). (C) The mitochondrial membrane potential was analyzed in different treatment groups using tetramethylrhodamine ethyl ester perchlorate staining (Mito-TEMPO, 200 μM; magnification, x200; scale bar, 100 μm; n=3). (D) The GSDMD-FL and GSDMD-N expression levels in different treatment groups were measured using western blotting assays (Mito-TEMPO, 200 μM; n=3). (E) The GSDMD-N expression levels were measured in different treatment groups using IF staining assays (Mito-TEMPO, 200 μM; magnification, x200; scale bar, 100 μm; n=3). (F) Western blotting assays were used to reveal the expression levels of NLRP3, Casp1-FL and cleaved-Casp1 in different treatment groups (Mito-TEMPO, 200 μM; n=3). (G) IF staining assays were used to measure the expression levels of NLRP3 and cleaved-Casp1 in different treatment groups (Mito-TEMPO, 200 μM; magnification, x200; scale bar, 100 μm; n=3). (H) ELISA assays were used to reveal the IL-1β and IL-18 protein levels in different treatment groups (Mito-TEMPO, 200 μM; n=3). *P<0.05 and **P<0.01. Con, control; H/R, hypoxia/reoxygenation; GSDMD, gasdermin D; GSDMD-FL, GSDMD-full length; GSDMD-N, GSDMD-N-terminal domain; NLRP3, NOD-, LRR- and pyrin domain-containing protein 3; IF, immunofluorescent; IL, interleukin; Casp1, caspase-1; Casp1-FL, Casp1-full length; ROS, reactive oxygen species.

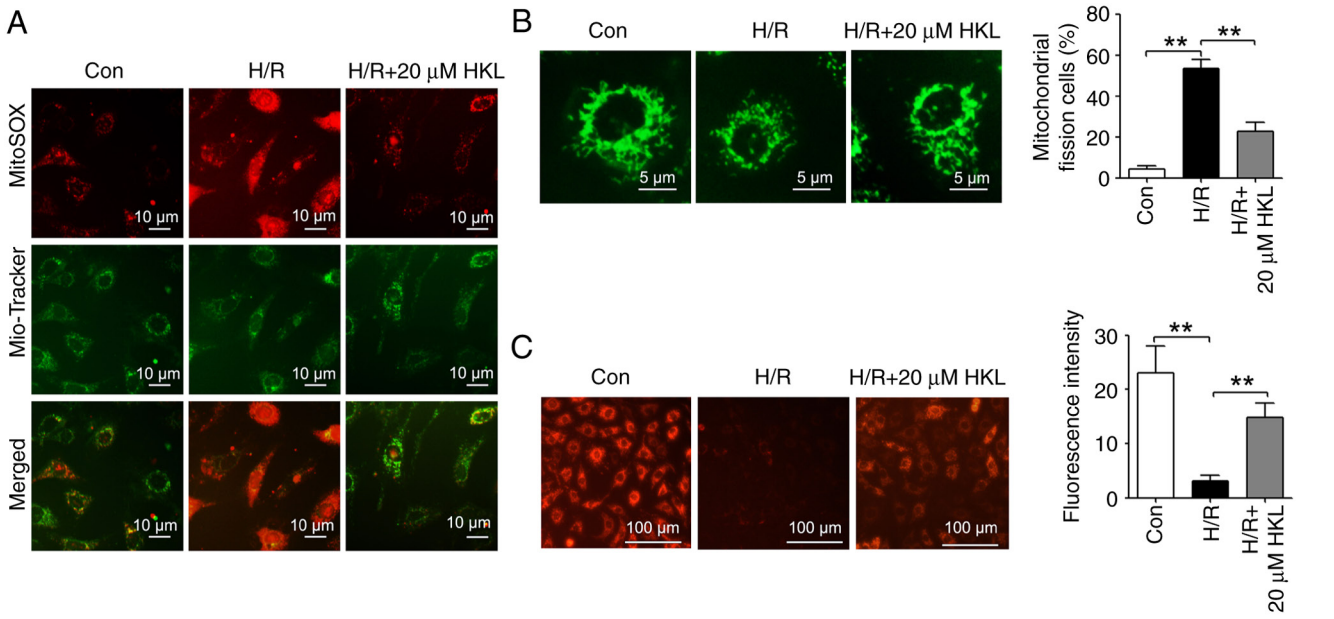

Figure 4. HKL reduces mitochondrial dysfunction in IEC-6 cells following H/R. (A) MitoSOX Red and Mito-Tracker Green co-staining was used to investigate the effect of HKL on the generation of mitochondrial reactive oxygen species in IEC-6 cells following H/R (magnification, x400; scale bar, 10 μm). (B) The effects of HKL on mitochondrial fission and integrity were demonstrated using Mito-Tracker Green staining in IEC-6 cells after H/R (magnification, x1,000; scale bar, 5 μm; n=3). (C) The mitochondrial membrane potential was analyzed in different treatment groups using tetramethylrhodamine ethyl ester perchlorate staining (magnification, x200; scale bar, 100 μm; n=3). **P<0.01. Con, control; H/R, hypoxia/reoxygenation; HKL, honokiol.

decreased the H/R-induced increases in the IL-1β and IL-18 levels in IEC-6 cells; however, SIRT3 knockdown significantly reversed the effect of HKL (Fig. 6E). Therefore, these results suggested that SIRT3 may be involved in the HKL-mediated pyroptosis inhibition in IEC-6 cells.

HKL alleviates IIR-induced pyroptosis by increasing the expression of SIRT3 protein in vivo. IHC staining experiments revealed that SIRT3 was significantly decreased in the intestinal tissues of IIR-induced rats compared with the sham group. However, 10 mg/kg HKL treatment significantly reversed this IIR-induced change (Fig. 7A and B). In addition, 10 mg/kg HKL treatment significantly reversed the IIR-induced changes in NLRP3, cleaved-Casp1 and GSDMD-N protein levels in the intestinal tissues of rats (Fig. 7A and B). Furthermore, western blotting assays indicated that, compared with the sham group, IIR significantly reduced the SIRT3 protein levels and significantly increased the NLRP3 protein levels as well as the cleaved-Casp1/Casp1-FL and GSDMD-N/GSDMD-FL ratios in the intestinal tissues of rats (Fig. 7C). However, 10 mg/kg HKL treatment significantly reversed these IIR-induced changes (Fig. 7C). Compared with the sham group, IIR significantly increased the serum IL-1β and IL-18 levels in rats; however, 10 mg/kg HKL treatment significantly reversed these IIR-induced effects (Fig. 7D). Taken together, these findings suggested that HKL may inhibit pyroptosis by regulating the expression of SIRT3 protein in IIR-induced injury.

Discussion

Previous studies indicate that HKL possesses protective functions against a number of ischemia-reperfusion injuries, such as myocardial ischemia-reperfusion injury, renal ischemia-reperfusion injury and brain ischemia-reperfusion injury (45,56,57). However, to the best of our knowledge, the present study was the first to investigate the role of HKL in IIR injury. In the present study, a rat IIR model was established, and the effect of HKL on IIR-induced injury was examined. It was revealed that, compared with IIR-induced injury alone, HKL pretreatment notably reduced the damage to the intestinal mucosa, the Chiu's score and the serum i-FABP concentration, and increased the levels of intestinal barrier proteins. To further investigate the effect of HKL on IIR-induced injury *in vitro*, a H/R cell model was created to mimic IIR-induced injury. HKL treatment ameliorated the H/R-induced decrease in the viability of IEC-6 cells and reversed the H/R-induced levels of LDH. Taken together, the present study indicated the beneficial role of HKL in IIR-induced injury; however, the detailed mechanisms need to be further investigated.

Under normal physiological conditions, pyroptosis serves a role in the resistance of pathogen infection (11). However, excessive pyroptosis occurs in a number of pathological processes, such as myocardial infarction and septicemia, and induces cell death and inflammatory responses (10). Accumulating evidence indicates that pyroptosis is associated with ischemia-reperfusion injury in different organs (58). For example, during cerebral ischemia-reperfusion injury, pyroptosis is induced in astrocytes and promotes inflammation, and suppressing pyroptosis improves sensorimotor function, spatial learning and memory function, and reduces infarct volume and brain edema (59). When IIR occurs, pyroptosis is also notably increased, whereas intestinal barrier disruption and cell death are reduced by inhibiting pyroptosis (23). In addition, HKL improves the aberrant interactions between tubular epithelial cells and renal resident macrophages by inhibiting pyroptosis in lupus nephritis (60). The results of the present

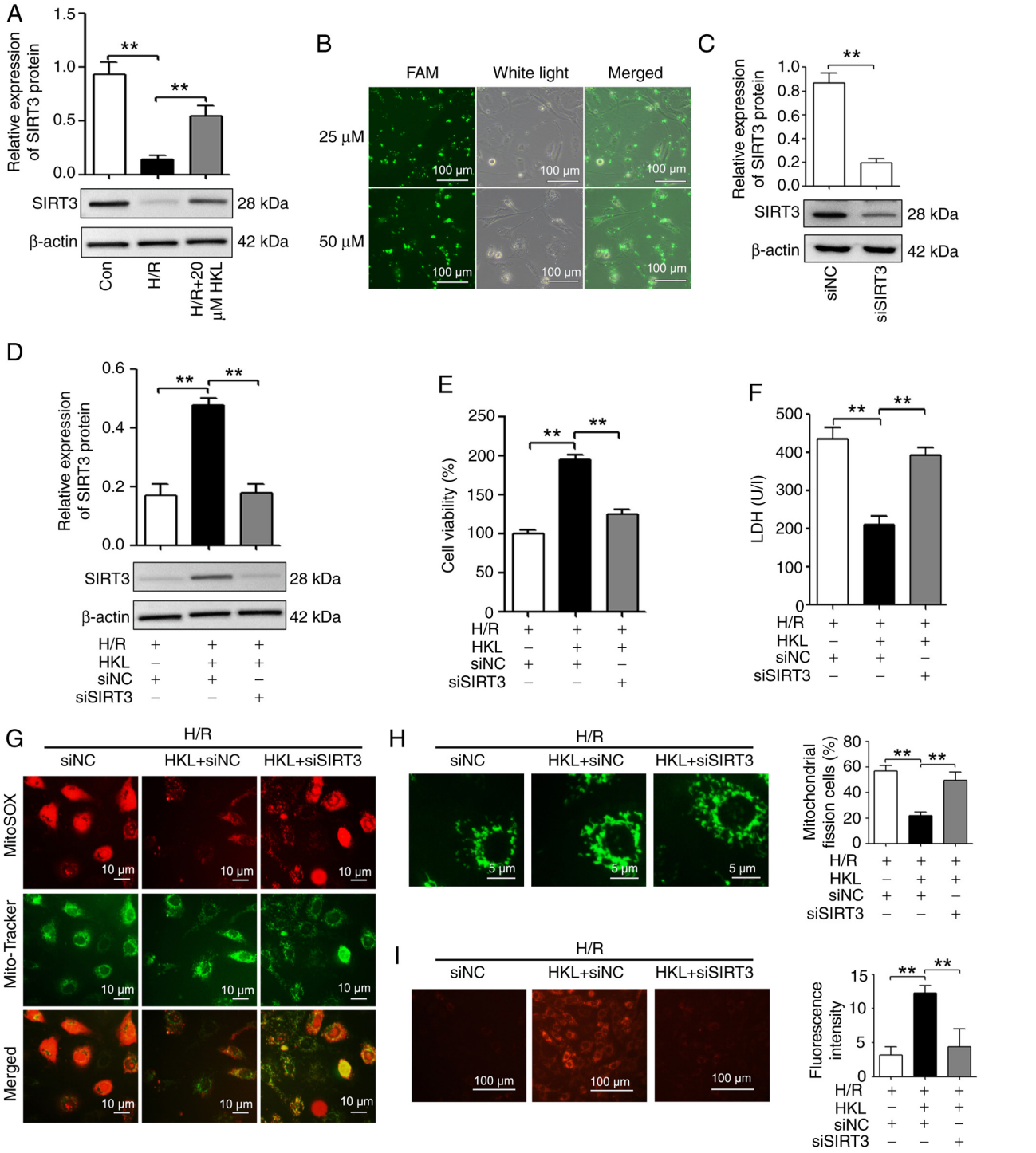

Figure 5. HKL (20 μM) reduces mitochondrial dysfunction by inducing SIRT3 in IEC-6 cells following H/R. (A) Western blotting was used to measure the SIRT3 expression levels in different treatment groups (n=3). (B) The transfection efficiency of siRNAs was demonstrated using FAM-labeled siNC (magnification, x200; scale bar, 100 μm). (C) The knockdown efficiency of siSIRT3 was revealed using western blotting (n=3). (D) Western blotting was used to demonstrate the effect of siSIRT3 on the SIRT3 levels in IEC-6 cells after exposure to H/R and HKL (n=3). (E) The cell viability of IEC-6 cells after different treatments was measured using a Cell Counting Kit-8 assay (n=3). (F) The cell injury of IEC-6 cells after different treatments was investigated by analyzing the LDH levels (n=3). (G) The generation of mitochondrial reactive oxygen species was revealed using MitoSOX Red and Mito-Tracker Green co-staining in IEC-6 cells after different treatments (magnification, x400; scale bar, 10 μm). (H) Mitochondrial fission and integrity were revealed using Mito-Tracker Green staining in H/R-induced IEC-6 cells following HKL and siSIRT3 treatment (magnification, x1,000; scale bar, 5 μm; n=3). (I) The mitochondrial membrane potential was analyzed in different treatment groups using tetramethylrhodamine ethyl ester perchlorate staining (magnification, x200; scale bar, 100 μm; n=3). **P<0.01. Con, control; H/R, hypoxia/reoxygenation; SIRT3, sirtuin 3; FAM, fluorescein amidite; LDH, lactate dehydrogenase; si, small interfering RNA; NC, negative control; HKL, honokiol.

study indicated that IIR induced pyroptosis, as evidenced by increased levels of GSDMD-N (a marker of pyroptosis). Therefore, it was hypothesized that HKL may ameliorate IIR-induced injury by inhibiting pyroptosis. The results of the present study revealed that HKL treatment inhibited the H/R-induced change in the GSDMD-N protein level. Under

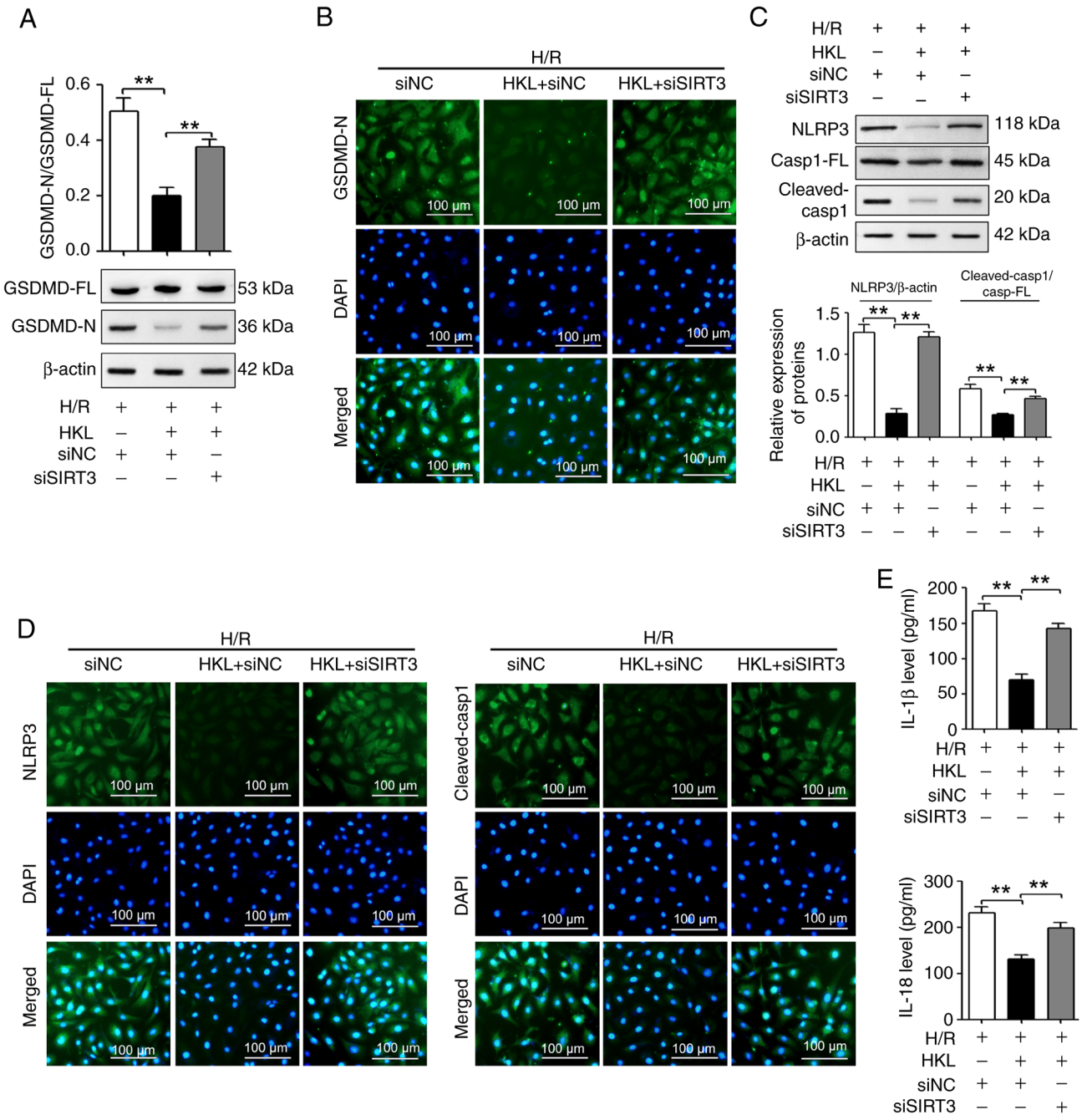

Figure 6. HKL (20 μM)reduces pyroptosis by increasing the SIRT3 protein levels in IEC-6 cells following H/R. (A) Western blotting revealed the GSDMD-FL and GSDMD-N protein levels (n=3). (B) The GSDMD-N protein levels were measured using immunofluorescent staining assays (magnification, x200; scale bar, 100 μm; n=3). (C) NLRP3, Casp1-FL and cleaved-Casp1 protein levels were revealed using western blotting assays (n=3). (D) NLRP3 and cleaved-Casp1 protein levels were measured using immunofluorescent staining assays in H/R-induced IEC-6 cells with different treatments (magnification, x200; scale bar, 100 μm; n=3). (E) ELISA assays were used to analyze the IL-1β and IL-18 protein levels in different treatment groups (n=3). **P<0.01. H/R, hypoxia/reoxygenation; SIRT3, sirtuin 3; si, small interfering RNA; NC, negative control; GSDMD, gasdermin D; GSDMD-FL, GSDMD-full length; GSDMD-N, GSDMD-N-terminal domain; NLRP3, NOD-, LRR- and pyrin domain-containing protein 3; IL, interleukin; Casp1, caspase-1; Casp1-FL, Casp1-full length; HKL, honokiol.

pathological conditions, including ischemia-reperfusion injury, the canonical pathway of pyroptosis involves the activation of the NLRP3 inflammasome, which increases cleaved-Casp1 production, resulting in the cleaving of pro-IL-18 and pro-IL-1β into their mature forms and the induction of pyroptosis (58,61). The present study revealed that H/R treatment increased the levels of NLRP3, cleaved-Casp1, IL-1β and IL-18 in IEC-6 cells, and that this change was reversed by HKL. Additionally, a study by Liu *et al* (50) reveals that HKL treatment improves acute lung injury by suppressing NLRP3 inflammasome-induced pyroptosis. These results indicated that HKL treatment may ameliorate IIR injury by reversing NLRP3 inflammasome-induced pyroptosis.

Mitochondrial damage and dysfunction are involved in IIR-induced injury (26,27,42). During IIR, mitochondrial dysfunction generates excessive ROS, and the increase in ROS induces mtDNA damage, which subsequently leads to increased ROS production and mitochondrial dysfunction,

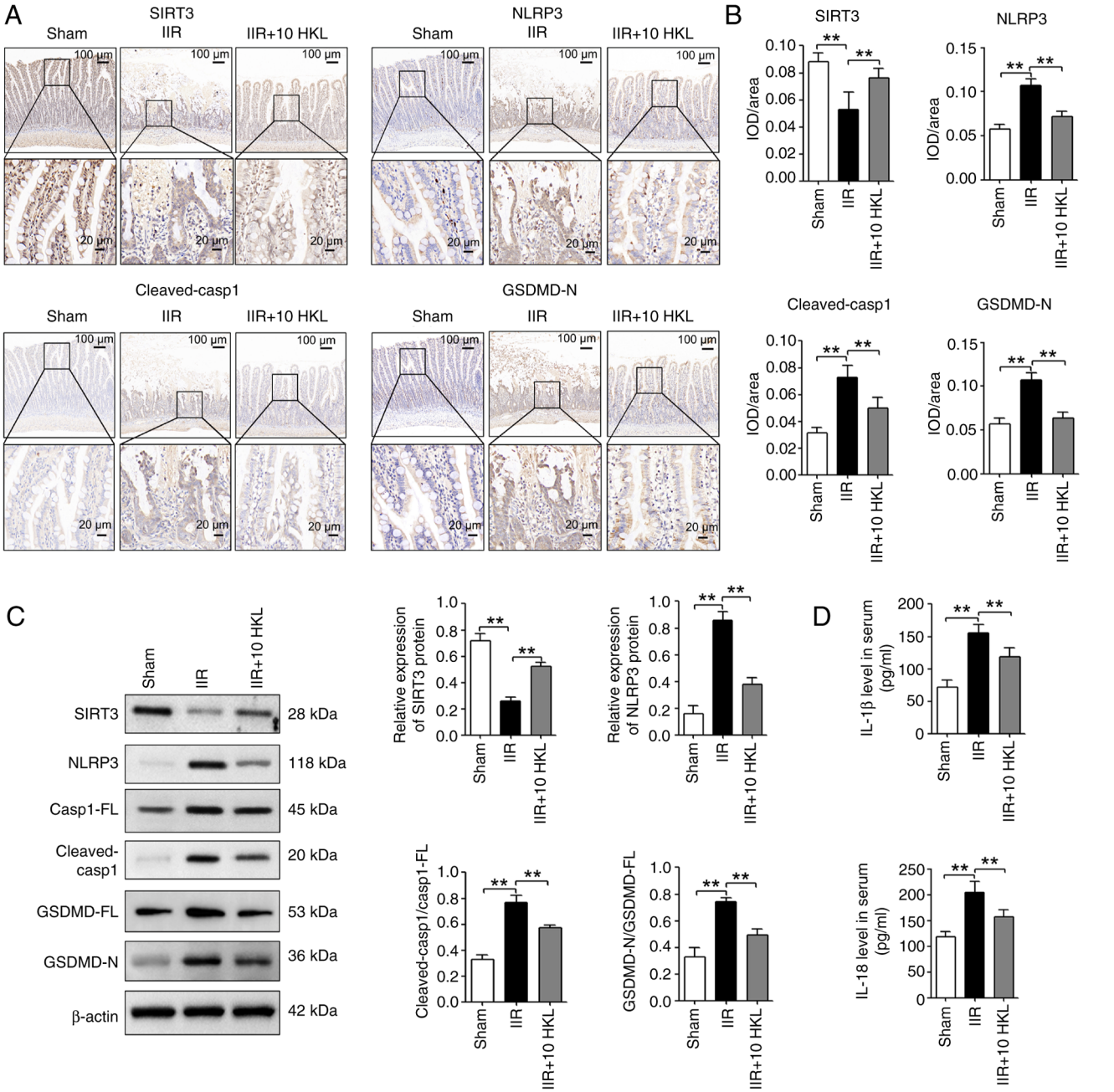

Figure 7. HKL (10 mg/kg) reduces IIR-induced pyroptosis by increasing the SIRT3 protein levels in rats. (A) SIRT3, NLRP3, cleaved-Casp1 and GSDMD-N protein levels were measured using immunohistochemical staining assays and consecutive sectioning of the same specimen in the same area of the intestinal tissues from different treatment groups (magnification, x100 or x400; scale bars, 100 or 20 μm; n=6). (B) Quantification of SIRT3, NLRP3, cleaved-Casp1 and GSDMD-N expression levels after immunohistochemical staining. (C) SIRT3, NLRP3, Casp1-FL, cleaved-Casp1, GSDMD-FL and GSDMD-N protein levels were revealed using western blotting in rats following IIR and 10 mg/kg HKL treatment (n=4). (D) Serum IL-1β and IL-18 levels were analyzed using ELISA assays in rats after IIR and 10 mg/kg HKL treatment (n=6). **P<0.01. HKL, honokiol; IIR, intestinal ischemia-reperfusion; SIRT3, sirtuin 3; GSDMD, gasdermin D; GSDMD-FL, GSDMD-full length; GSDMD-N, GSDMD-N-terminal domain; NLRP3, NOD-, LRR- and pyrin domain-containing protein 3; IL, interleukin; Casp1, caspase-1; Casp1-FL, Casp1-full length; IOD, integrated optical density.

thereby inducing cell death (26). Evidence suggests that the overproduction of ROS by damaged mitochondria can induce pyroptosis (62). The results of the present study indicated that inhibiting mitochondrial ROS reduced the H/R-induced mitochondrial fission and reduction of the $\Delta\psi_m$. Therefore, this indicated that mitochondrial ROS inhibition may improve IIR-induced pyroptosis. The results of the present study revealed that reducing mitochondrial ROS production with Mito-TEMPO reduced pyroptosis, which was evidenced by decreased NLRP3, cleaved-Casp1 and GSDMD-N protein levels, as well as reduced IL-1β and IL-18 levels. Consistent with these results, phospholipase C ε1 promotes cardiomyocyte pyroptosis by inducing defective mitochondrial function in doxorubicin-induced cardiotoxicity (63). To the best of our knowledge, the present study was the first to provide evidence that mitochondrial dysfunction may be involved in pyroptosis during IIR-induced injury.

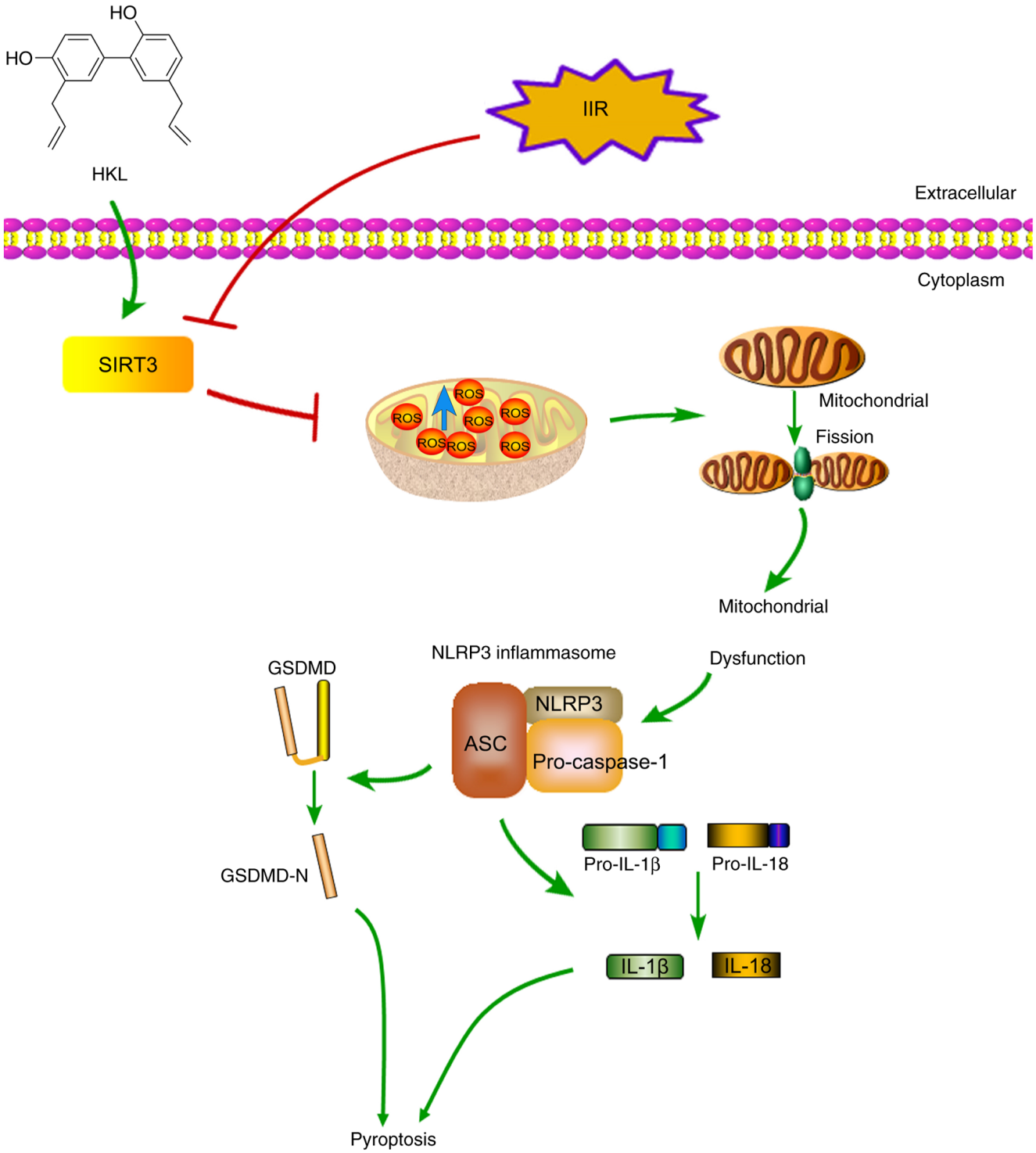

Figure 8. Schematic diagram of the suggested protective mechanism of HKL on IIR-induced injury in rats. HKL inhibited IIR-induced pyroptosis by alleviating mitochondrial dysfunction through the upregulation of SIRT3 protein expression levels. HKL, honokiol; SIRT3, sirtuin 3; GSDMD, gasdermin D; GSDMD-N, GSDMD-N-terminal domain; NLRP3, NOD-, LRR- and pyrin domain-containing protein 3; IL, interleukin; ROS, reactive oxygen species; ASC, apoptosis-associated speck-like protein; IIR, intestinal ischemia-reperfusion.

Since ROS production induced by mitochondrial dysfunction can induce pyroptosis, drugs that protect mitochondrial function may inhibit ROS-induced pyroptosis. HKL has a protective role in a number of pathological processes by mitigating mitochondrial dysfunction (45,64). For example, HKL exerts cardioprotection by inhibiting mitochondrial dysfunction-induced apoptosis in myocardial ischemia-reperfusion injury (45). Therefore, it was hypothesized that HKL may reduce ROS-induced pyroptosis by improving mitochondrial dysfunction in IIR-induced injury. In the present study, the results of the *in vitro* experiments provided evidence to support this hypothesis. HKL treatment notably alleviated H/R-induced mitochondrial fission, reduced mitochondrial ROS production and reversed the reduction of the $\Delta\psi_m$.

Finally, the results of the present study suggested that the SIRT3/NLRP3 pathway may be important for HKL mediated-pyroptosis in IIR injury. SIRT3, a mitochondrial deacetylase, is involved in regulating mitochondrial function, cellular energy homeostasis and mitochondrial ROS production (56,65-67). In a number of ischemia-reperfusion injuries, including IIR injury, SIRT3 expression levels are reduced; however, increasing the SIRT3 expression levels ameliorates ischemia-reperfusion injury by preserving mitochondrial function and reducing mitochondrial ROS production (68-70). A recent study reveals that SIRT3 activation by Liguzinediol alleviates gasdermin E-mediated pyroptosis by suppressing mitochondrial ROS production, which inhibits doxorubicin-associated cardiotoxicity (71). In the progression of atherosclerosis, melatonin inhibits NLRP3 inflammasome-mediated macrophage pyroptosis by decreasing ROS production by activating the SIRT3/Forkhead box O3 pathway (72). In trimethylamine-N-oxide-induced vascular inflammation, the downregulation of SIRT3 leads to mitochondrial ROS production by suppressing the activation of superoxide dismutase 2, which results in NLRP3 inflammasome-mediated pyroptosis (73). Additionally, results from molecular docking reveal that HKL can directly bind to SIRT3 protein with a low binding energy (-4.45 kcal mol^{-1}) at GLU371 and THR380 (74). HKL can bind to SIRT3 and promote SIRT3 deacetylase activity by increasing its affinity for NAD, which reduces the acetylation of manganese-containing superoxide dismutase and reverses ROS synthesis and cardiac hypertrophy in mice (38).

As HKL can inhibit NLRP3 inflammasome-mediated pyroptosis by ameliorating mitochondrial dysfunction-induced mitochondrial ROS production during IIR-induced injury, it was hypothesized that HKL would inhibit IIR-induced pyroptosis by regulating the SIRT3/ROS axis. In the present study, HKL treatment notably increased the levels of SIRT3 after the H/R and IIR-induced SIRT3 downregulation *in vitro* and *in vivo*. In addition, knocking down SIRT3 using siRNA reduced the protective effects of HKL on the viability and mitochondrial dysfunction of IEC-6 cells. Knocking down SIRT3 also reversed the HKL-induced reductions in the LDH levels and mitochondrial ROS production. Furthermore, silencing SIRT3 in the present H/R model reversed the HKL-induced reductions of GSDMD-N, NLRP3 and cleaved-Casp1 as well as the reduced IL-1β and IL-18 levels. Therefore, these data indicated that the SIRT3/NLRP3 pathway may be important for the HKL mediated pyroptosis inhibition in IIR injury.

The findings of the present study, as well as those of previous studies, indicated that the SIRT3 protein levels were increased following HKL treatment (40,75,76). In addition, a previous study revealed that treatment with HKL also increased the mRNA expression of SIRT3 during cardiac hypertrophy (38). The results of the present study also revealed that HKL treatment increased the SIRT3 mRNA levels in IEC-6 cells after H/R inhibition. The mechanism underlying the HKL-induced increase to the SIRT3 mRNA levels remains unclear, which was a limitation of the present study. Previous studies indicate that nuclear factor erythroid 2-related factor 2 (Nrf2)-induced SIRT3 mRNA transcription is involved in alleviating mitochondrial dysfunction in stress conditions (77,78). In acute lung injury, HKL reverses the LPS-induced inhibition of Nrf2, which reduces oxidative stress and pyroptosis (47). Therefore, these findings indicated that HKL may promote SIRT3 mRNA transcription by regulating Nrf2. In addition, HKL maintains the post-translational activation of SIRT3 and upregulates the SIRT3 mRNA level by activating peroxisome proliferator-activated receptor-γ coactivator-1α in cardiac hypertrophy (38). Therefore, to further investigate the positive feedback mechanism regulating SIRT3 mRNA transcription, an in-depth study is required. Another limitation of the present study is that the mechanism of the SIRT3-regulated mitochondrial dysfunction and mitochondrial ROS production in IIR injury also remains unclear. The underlying regulatory mechanism should be investigated in future studies.

In conclusion, the present study was, to the best of our knowledge, the first to indicate that IIR-induced mitochondrial dysfunction triggered pyroptosis via the NLRP3 axis, and that HKL treatment may have protective effects by upregulating SIRT3 and alleviating mitochondrial dysfunction (Fig. 8).

Acknowledgements

Not applicable.

Funding

This study was supported by the Sichuan Provincial Administration of Traditional Chinese Medicine 2023 Traditional Chinese Medicine Research Special Project (grant no. 2023MS038), the Sichuan Provincial Administration of Traditional Chinese Medicine 2024 Traditional Chinese Medicine Research Special Project (grant no. 2024MS151) and the Southwest Medical University Integrated Traditional Chinese and Western Medicine Special Project (grant no. 2023ZYYJ07).

Availability of data and materials

The data generated in the present study may be requested from the corresponding author.

Authors' contributions

KW, CX and WG designed the study. KW, ZZ, QW and WG performed the animal experiments. KW, WL, JP, LW and WG performed the cell experiments. KW, CX, WL, JP and XM analyzed data. KW, CX and WG wrote the first draft of the manuscript. WL, JP, ZZ, QW, CX, LW, XM and WG revised the manuscript. KW, CX and WG confirm the authenticity of all the raw data. All authors read and approved the final version of the manuscript.

Ethics approval and consent to participate

The animal experimental protocols were approved by the Ethics Committee of Southwest Medical University (Luzhou, China; approval no. 20221128-001).

Patient consent for publication

Not applicable.

Competing interests

The authors declare that they have no competing interests.

References

1. Jin B, Li G, Zhou L and Fan Z: Mechanism involved in acute liver injury induced by intestinal Ischemia-reperfusion. Front Pharmacol 13: 924695, 2022.
2. Tassopoulos A, Chalkias A, Papalois A, Iacovidou N and Xanthos T: The effect of antioxidant supplementation on bacterial translocation after intestinal ischemia and reperfusion. Redox Rep 22: 1-9, 2017.
3. Taylor LM Jr and Moneta GL: Intestinal ischemia. Ann Vasc Surg 5: 403-406, 1991.
4. Slone EA and Fleming SD: Membrane lipid interactions in intestinal ischemia/reperfusion-induced Injury. Clin Immunol 153: 228-240, 2014.
5. Stamatakos M, Stefanaki C, Mastrokalos D, Arampatzi H, Safioleas P, Chatziconstantinou C, Xiromeritis C and Safioleas M: Mesenteric ischemia: Still a deadly puzzle for the medical community. Tohoku J Exp Med 216: 197-204, 2008.
6. Li G, Wang S and Fan Z: Oxidative stress in intestinal ischemia-reperfusion. Front Med (Lausanne) 8: 750731, 2022.
7. Zhang X, Wu J, Liu Q, Li X, Li S, Chen J, Hong Z, Wu X, Zhao Y and Ren J: mtDNA-STING pathway promotes necroptosis-dependent enterocyte injury in intestinal ischemia reperfusion. Cell Death Dis 11: 1050, 2020.
8. Subramanian S, Geng H and Tan XD: Cell death of intestinal epithelial cells in intestinal diseases. Sheng Li Xue Bao 72: 308-324, 2020.
9. Li Y, Feng D, Wang Z, Zhao Y, Sun R, Tian D, Liu D, Zhang F, Ning S, Yao J and Tian X: Ischemia-induced ACSL4 activation contributes to ferroptosis-mediated tissue injury in intestinal ischemia/reperfusion. Cell Death Differ 26: 2284-2299, 2019.
10. Wei Y, Yang L, Pandeya A, Cui J, Zhang Y and Li Z: Pyroptosis-induced inflammation and tissue damage. J Mol Biol 434: 167301, 2022.
11. Rao Z, Zhu Y, Yang P, Chen Z, Xia Y, Qiao C, Liu W, Deng H, Li J, Ning P, *et al*: Pyroptosis in inflammatory diseases and cancer. Theranostics 12: 4310-4329, 2022.
12. Ji X, Tian L, Niu S, Yao S and Qu C: Trimethylamine N-oxide promotes demyelination in spontaneous hypertension rats through enhancing pyroptosis of oligodendrocytes. Front Aging Neurosci 14: 963876, 2022.
13. Wang Y, Chen J, Zheng Y, Jiang J, Wang L, Wu J, Zhang C and Luo M: Glucose metabolite methylglyoxal induces vascular endothelial cell pyroptosis via NLRP3 inflammasome activation and oxidative stress in vitro and in vivo. Cell Mol Life Sci 81: 401, 2024.
14. Vasudevan SO, Behl B and Rathinam VA: Pyroptosis-induced inflammation and tissue damage. Semin Immunol 69: 101781, 2023.
15. Guo Q, Wu Y, Hou Y, Liu Y, Liu T, Zhang H, Fan C, Guan H, Li Y, Shan Z and Teng W: Cytokine secretion and pyroptosis of thyroid follicular cells mediated by enhanced NLRP3, NLRP1, NLRC4, and AIM2 inflammasomes are associated with autoimmune thyroiditis. Front Immunol 9: 1197, 2018.
16. Karki R, Sharma BR, Tuladhar S, Williams EP, Zalduondo L, Samir P, Zheng M, Sundaram B, Banoth B, Malireddi RKS, *et al*: Synergism of TNF-α and IFN-γ triggers inflammatory cell death, tissue damage, and mortality in SARS-CoV-2 infection and cytokine shock syndromes. Cell 184: 149-168.e17, 2021.
17. Li Y, Yuan Y, Huang ZX, Chen H, Lan R, Wang Z, Lai K, Chen H, Chen Z, Zou Z, *et al*: GSDME-mediated pyroptosis promotes inflammation and fibrosis in obstructive nephropathy. Cell Death Differ 28: 2333-2350, 2021.
18. Coll RC, Schroder K and Pelegrín P: NLRP3 and pyroptosis blockers for treating inflammatory diseases. Trends Pharmacol Sci 43: 653-668, 2022.
19. Bai B, Yang Y, Wang Q, Li M, Tian C, Liu Y, Aung LHH, Li PF, Yu T and Chu XM: NLRP3 inflammasome in endothelial dysfunction. Cell Death Dis 11: 776, 2020.
20. Huang Y, Xu W and Zhou R: NLRP3 inflammasome activation and cell death. Cell Mol Immunol 18: 2114-2127, 2021.
21. Zhang L, Ai C, Bai M, Niu J and Zhang Z: NLRP3 Inflammasome/Pyroptosis: A key driving force in diabetic cardiomyopathy. Int J Mol Sci 23: 10632, 2022.
22. Kovacs SB and Miao EA: Gasdermins: Effectors of pyroptosis. Trends Cell Biol 27: 673-684, 2017.
23. Jia Y, Cui R, Wang C, Feng Y, Li Z, Tong Y, Qu K, Liu C and Zhang J: Metformin protects against intestinal ischemia-reperfusion injury and cell pyroptosis via TXNIP-NLRP3-GSDMD pathway. Redox Biol 32: 101534, 2020.
24. Li W, Yang K, Li B, Wang Y, Liu J, Chen D and Diao Y: Corilagin alleviates intestinal ischemia/reperfusion-induced intestinal and lung injury in mice via inhibiting NLRP3 inflammasome activation and pyroptosis. Front Pharmacol 13: 1060104, 2022.
25. Chen Y, Han B, Guan X, Du G, Sheng B, Tang X, Zhang Q, Xie H, Jiang X, Tan Q, *et al*: Enteric fungi protect against intestinal ischemia-reperfusion injury via inhibiting the SAA1-GSDMD pathway. J Adv Res 61: 223-237, 2024.
26. Hu Q, Ren J, Li G, Wu J, Wu X, Wang G, Gu G, Ren H, Hong Z and Li J: The mitochondrially targeted antioxidant MitoQ protects the intestinal barrier by ameliorating mitochondrial DNA damage via the Nrf2/ARE signaling pathway. Cell Death Dis 9: 403, 2018.
27. Liao S, Luo J, Kadier T, Ding K, Chen R and Meng Q: Mitochondrial DNA release contributes to intestinal ischemia/reperfusion injury. Front Pharmacol 13: 854994, 2022.
28. Zhang Y, Lv Y, Zhang Q, Wang X, Han Q, Liang Y, He S, Yuan Q, Zheng J, Xu C, *et al*: ALDH2 attenuates myocardial pyroptosis through breaking down Mitochondrion-NLRP3 inflammasome pathway in septic shock. Front Pharmacol 14: 1125866, 2023.
29. Cheon SY, Kim MY, Kim J, Kim EJ, Kam EH, Cho I, Koo BN and Kim SY: Hyperammonemia induces microglial NLRP3 inflammasome activation via mitochondrial oxidative stress in hepatic encephalopathy. Biomed J 46: 100593, 2023.
30. Li Z, Wang B, Tian L, Zheng B, Zhao X and Liu R: Methane-rich saline suppresses ER-mitochondria contact and activation of the NLRP3 inflammasome by regulating the PERK signaling pathway to ameliorate intestinal Ischemia-reperfusion injury. Inflammation 47: 376-389, 2024.
31. Mao H, Zhang Y, Xiong Y, Zhu Z, Wang L and Liu X: Mitochondria-targeted antioxidant mitoquinone maintains mitochondrial homeostasis through the Sirt3-dependent pathway to mitigate oxidative damage caused by renal ischemia/reperfusion. Oxid Med Cell Longev 2022: 2213503, 2022.
32. Zhang Q, Liu XM, Hu Q, Liu ZR, Liu ZY, Zhang HG, Huang YL, Chen QH, Wang WX and Zhang XK: Dexmedetomidine inhibits mitochondria damage and apoptosis of enteric glial cells in experimental intestinal ischemia/reperfusion injury via SIRT3-dependent PINK1/HDAC3/p53 pathway. J Transl Med 19: 463, 2021.
33. Shen X, Shi H, Chen X, Han J, Liu H, Yang J, Shi Y and Ma J: Esculetin alleviates inflammation, oxidative stress and apoptosis in intestinal ischemia/reperfusion injury via targeting SIRT3/AMPK/mTOR signaling and regulating autophagy. J Inflamm Res 16: 3655-3667, 2023.
34. Wang Z, Sun R, Wang G, Chen Z, Li Y, Zhao Y, Liu D, Zhao H, Zhang F, Yao J, *et al*: SIRT3-mediated deacetylation of PRDX3 alleviates mitochondrial oxidative damage and apoptosis induced by intestinal ischemia/reperfusion injury. Redox Biol 28: 101343, 2020.
35. Chen HH, Chang PC, Chen C and Chan MH: Protective and therapeutic activity of honokiol in reversing motor deficits and neuronal degeneration in the mouse model of Parkinson's disease. Pharmacol Rep 70: 668-676, 2018.
36. Huang K, Chen Y, Zhang R, Wu Y, Ma Y, Fang X and Shen S: Honokiol induces apoptosis and autophagy via the ROS/ERK1/2 signaling pathway in human osteosarcoma cells in vitro and in vivo. Cell Death Dis 9: 157, 2018.
37. Zhou Y, Tang J, Lan J, Zhang Y, Wang H, Chen Q, Kang Y, Sun Y, Feng X, Wu L, *et al*: Honokiol alleviated neurodegeneration by reducing oxidative stress and improving mitochondrial function in mutant SOD1 cellular and mouse models of amyotrophic lateral sclerosis. Acta Pharm Sin B 13: 577-597, 2023.
38. Pillai VB, Samant S, Sundaresan NR, Raghuraman H, Kim G, Bonner MY, Arbiser JL, Walker DI, Jones DP, Gius D and Gupta MP: Honokiol blocks and reverses cardiac hypertrophy in mice by activating mitochondrial Sirt3. Nat Commun 6: 6656, 2015.
39. Zhang Y, Wen P, Luo J, Ding H, Cao H, He W, Zen K, Zhou Y, Yang J and Jiang L: Sirtuin 3 regulates mitochondrial protein acetylation and metabolism in tubular epithelial cells during renal fibrosis. Cell Death Dis 12: 847, 2021.
40. Mao RW, He SP, Lan JG and Zhu WZ: Honokiol ameliorates cisplatin-induced acute kidney injury via inhibition of mitochondrial fission. Br J Pharmacol 179: 3886-3904, 2022.

41. Gao Y, Chen H, Cang X, Chen H, Di Y, Qi J, Cai H, Luo K and Jin S: Transplanted hair follicle mesenchymal stem cells alleviated small intestinal ischemia-reperfusion injury via intrinsic and paracrine mechanisms in a rat model. Front Cell Dev Biol 10: 1016597, 2022.
42. Almoiliqy M, Wen J, Xu B, Sun YC, Lian MQ, Li YL, Qaed E, Al-Azab M, Chen DP, Shopit A, *et al*: Cinnamaldehyde protects against rat intestinal ischemia/reperfusion injuries by synergistic inhibition of NF-κB and p53. Acta Pharmacol Sin 41: 1208-1222, 2020.
43. Zhang B, Zhai M, Li B, Liu Z, Li K, Jiang L, Zhang M, Yi W, Yang J, Yi D, *et al*: Honokiol ameliorates myocardial ischemia/reperfusion injury in type 1 diabetic rats by reducing oxidative stress and apoptosis through activating the SIRT1-Nrf2 signaling pathway. Oxid Med Cell Longev 2018: 3159801, 2018.
44. Zheng J, Shi L, Liang F, Xu W, Li T, Gao L, Sun Z, Yu J and Zhang J: Sirt3 ameliorates oxidative stress and mitochondrial dysfunction after intracerebral hemorrhage in diabetic rats. Front Neurosci 12: 414, 2018.
45. Lv L, Kong Q, Li Z, Zhang Y, Chen B, Lv L and Zhang Y: Honokiol provides cardioprotection from myocardial ischemia/reperfusion injury (MI/RI) by inhibiting mitochondrial apoptosis via the PI3K/AKT signaling pathway. Cardiovasc Ther 2022: 1001692, 2022.
46. Cong R, Sun L, Yang J, Cui H, Ji X, Zhu J, Gu JH and He B: Protein O-GlcNAcylation alleviates small intestinal injury induced by ischemia-reperfusion and oxygen-glucose deprivation. Biomed Pharmacother 138: 111477, 2021.
47. Han X, Yao W, Liu Z, Li H, Zhang ZJ, Hei Z and Xia Z: Lipoxin A4 preconditioning attenuates intestinal ischemia reperfusion injury through keap1/Nrf2 pathway in a lipoxin A4 receptor independent manner. Oxid Med Cell Longev 2016: 9303606, 2016.
48. Livak KJ and Schmittgen TD: Analysis of relative gene expression data using real-time quantitative PCR and the 2(-Delta Delta C(T)) method. Methods 25: 402-408, 2001.
49. Li Y, Xu B, Xu M, Chen D, Xiong Y, Lian M, Sun Y, Tang Z, Wang L, Jiang C and Lin Y: 6-Gingerol protects intestinal barrier from ischemia/reperfusion-induced damage via inhibition of p38 MAPK to NF-κB signalling. Pharmacol Res 119: 137-148, 2017.
50. Liu Y, Zhou J, Luo Y, Li J, Shang L, Zhou F and Yang S: Honokiol alleviates LPS-induced acute lung injury by inhibiting NLRP3 inflammasome-mediated pyroptosis via Nrf2 activation in vitro and in vivo. Chin Med 16: 127, 2021.
51. Qiu L, Xu R, Wang S, Li S, Sheng H, Wu J and Qu Y: Honokiol ameliorates endothelial dysfunction through suppression of PTX3 expression, a key mediator of IKK/IκB/NF-κB, in atherosclerotic cell model. Exp Mol Med 47: e171, 2015.
52. Wang Y, Shi P, Chen Q, Huang Z, Zou D, Zhang J, Gao X and Lin Z: Mitochondrial ROS promote macrophage pyroptosis by inducing GSDMD oxidation. J Mol Cell Biol 11: 1069-1082, 2019.
53. Zheng Z, Bian Y, Zhang Y, Ren G and Li G: Metformin activates AMPK/SIRT1/NF-κB pathway and induces mitochondrial dysfunction to drive caspase3/GSDME-mediated cancer cell pyroptosis. Cell Cycle 19: 1089-1104, 2020.
54. Feng WQ, Zhang YC, Xu ZQ, Yu SY, Huo JT, Tuersun A, Zheng MH, Zhao JK, Zong YP and Lu AG: IL-17A-mediated mitochondrial dysfunction induces pyroptosis in colorectal cancer cells and promotes CD8 + T-cell tumour infiltration. J Transl Med 21:335, 2023.
55. Zhang J, Xiang H, Liu J, Chen Y, He RR and Liu B: Mitochondrial Sirtuin 3: New emerging biological function and therapeutic target. Theranostics 10: 8315-8342, 2020.
56. Park EJ, Dusabimana T, Je J, Jeong K, Yun SP, Kim HJ, Kim H and Park SW: Honokiol protects the kidney from renal ischemia and reperfusion injury by upregulating the glutathione biosynthetic enzymes. Biomedicines 8: 352, 2020.
57. Xu G, Dong R, Liu J, Zhao L, Zeng Y, Xiao X, An J, Huang S, Zhong Y, Guang B and Yang T: Synthesis, characterization and in vivo evaluation of honokiol bisphosphate prodrugs protects against rats' brain ischemia-reperfusion injury. Asian J Pharm Sci 14: 640-648, 2019.
58. Zheng Y, Xu X, Chi F and Cong N: Pyroptosis: A newly discovered therapeutic target for ischemia-reperfusion injury. Biomolecules 12: 1625, 2022.
59. Li J, Xu P, Hong Y, Xie Y, Peng M, Sun R, Guo H, Zhang X, Zhu W, Wang J and Liu X: Lipocalin-2-mediated astrocyte pyroptosis promotes neuroinflammatory injury via NLRP3 inflammasome activation in cerebral ischemia/reperfusion injury. J Neuroinflammation 20: 148, 2023.
60. Ma Q, Xu M, Jing X, Qiu J, Huang S, Yan H, Yin L, Lou J, Zhao L, Fan Y and Qiu P: Honokiol suppresses the aberrant interactions between renal resident macrophages and tubular epithelial cells in lupus nephritis through the NLRP3/IL-33/ST2 axis. Cell Death Dis 14: 174, 2023.
61. Feng Y, Li M, Yangzhong X, Zhang X, Zu A, Hou Y, Li L and Sun S: Pyroptosis in inflammation-related respiratory disease. J Physiol Biochem 78:721-737, 2022.
62. Zheng D, Liu J, Piao H, Zhu Z, Wei R and Liu K: ROS-triggered endothelial cell death mechanisms: Focus on pyroptosis, parthanatos, and ferroptosis. Front Immunol 13: 1039241, 2022.
63. Tuersuntuoheti M, Peng F, Li J, Zhou L, Gao H and Gong H: PLCE1 enhances mitochondrial dysfunction to promote GSDME-mediated pyroptosis in doxorubicin-induced cardiotoxicity. Biochem Pharmacol 223:116142, 2024.
64. Kerr M, Miller JJ, Thapa D, Stiewe S, Timm KN, Aparicio CNM, Scott I, Tyler DJ and Heather LC: Rescue of myocardial energetic dysfunction in diabetes through the correction of mitochondrial hyperacetylation by honokiol. JCI Insight 5: e140326, 2020.
65. Ji Z, Liu GH and Qu J: Mitochondrial sirtuins, metabolism, and aging. J Genet Genomics 49: 287-298, 2022.
66. Dikalov S and Dikalova A: Mitochondrial deacetylase Sirt3 in vascular dysfunction and hypertension. Curr Opin Nephrol Hypertens 31: 151-156, 2022.
67. Shen Y, Wu Q, Shi J, Zhou S: Regulation of SIRT3 on mitochondrial functions and oxidative stress in Parkinson's disease. Biomed Pharmacother 132: 110928, 2020.
68. Wang X, Shen T, Lian J, Deng K, Qu C, Li E, Li G, Ren Y, Wang Z, Jiang Z, *et al*: Resveratrol reduces ROS-induced ferroptosis by activating SIRT3 and compensating the GSH/GPX4 pathway. Mol Med 29: 137, 2023.
69. Xie X, Xu Q, Zhou D: Sirtuin-3 activates the mitochondrial unfolded protein response and reduces cerebral ischemia/reperfusion injury. Int J Biol Sci 19: 4327-4339, 2023.
70. Zhao H, Luo Y, Chen L, Zhang Z, Shen C, Li Y and Xu R: Sirt3 inhibits cerebral ischemia-reperfusion injury through normalizing Wnt/β-catenin pathway and blocking mitochondrial fission. Cell Stress Chaperones 23: 1079-1092, 2018.
71. Zhu W, Lian N, Wang J, Zhao F, Liu B, Sheng J, Zhang C, Zhou X, Gao W, Xie C, *et al*: Liguzinediol potentiates the metabolic remodeling by activating the AMPK/SIRT3 pathway and represses Caspase-3/GSDME-mediated pyroptosis to ameliorate cardiotoxicity. Chin Med 19: 85, 2024.
72. Cong L, Liu X, Bai Y, Qin Q, Zhao L, Shi Y, Bai Y and Guo Z: Melatonin alleviates pyroptosis by regulating the SIRT3/FOXO3α/ROS axis and interacting with apoptosis in Atherosclerosis progression. Biol Res 56: 62, 2023.
73. Chen ML, Zhu XH, Ran L, Lang HD, Yi L and Mi MT: Trimethylamine-N-Oxide induces vascular inflammation by activating the NLRP3 inflammasome through the SIRT3-SOD2-mtROS signaling pathway. J Am Heart Assoc 6: e006347, 2017.
74. Zhang Y, Liu Y, Hou M, Xia X, Liu J, Xu Y, Shi Q, Zhang Z, Wang L, Shen Y, *et al*: Reprogramming of Mitochondrial Respiratory Chain Complex by Targeting SIRT3-COX4I2 Axis Attenuates Osteoarthritis Progression. Adv Sci (Weinh) 10: e2206144, 2023.
75. Chang Y, Wang C, Zhu J, Zheng S, Sun S, Wu Y, Jiang X, Li L, Ma R and Li G: SIRT3 ameliorates diabetes-associated cognitive dysfunction via regulating mitochondria-associated ER membranes. J Transl Med 21: 494, 2023.
76. Zheng X, Gao J, Zhao M, Han L, Zhang D, Wang K and Cui J: Honokiol attenuates mitochondrial fission and cell apoptosis by activating Sirt3 in intracerebral hemorrhage. Chin Med J (Engl) 136: 719-731, 2023.
77. Yao Y, Ren Z, Yang R, Mei Y, Dai Y, Cheng Q, Xu C, Xu X, Wang S, Kim KM, *et al*: Salidroside reduces neuropathology in Alzheimer's disease models by targeting NRF2/SIRT3 pathway. Cell Biosci 12: 180, 2022.
78. Li Y, Feng L, Xie D, Luo Y, Lin M, Gao J, Zhang Y, He Z, Zhu YZ and Gong Q: Icariside II mitigates myocardial infarction by balancing mitochondrial dynamics and reducing oxidative stress through the activation of Nrf2/SIRT3 signaling pathway. Eur J Pharmacol 956: 175987, 2023.